Atmospheric Environment 43 (2009) 2229–2246

Contents lists available at ScienceDirect

Atmospheric Environment

journal homepage: www.elsevier.com/locate/atmosenv

Review

Photocatalytic purification of volatile organic compounds in indoor air: A literature review

Jinhan Mo [a], Yinping Zhang [a,*], Qiujian Xu [a], Jennifer Joaquin Lamson [a,b], Rongyi Zhao [a]

[a] Department of Building Science, Tsinghua University, Beijing 100084, PR China
[b] Department of Energy and Environment Engineering, Oslo University College, Norway

ARTICLE INFO

Article history:
Received 15 October 2008
Received in revised form
24 January 2009
Accepted 25 January 2009

Keywords:
Indoor air quality (IAQ)
Volatile organic compounds (VOCs)
Photocatalytic oxidation (PCO)
Air cleaning

ABSTRACT

Volatile organic compounds (VOCs) are prevalent components of indoor air pollution. Among the approaches to remove VOCs from indoor air, photocatalytic oxidation (PCO) is regarded as a promising method. This paper is a review of the status of research on PCO purification of VOCs in indoor air. The review and discussion concentrate on the preparation and coating of various photocatalytic catalysts; different kinetic experiments and models; novel methods for measuring kinetic parameters; reaction pathways; intermediates generated by PCO; and an overview of various PCO reactors and their models described in the literature. Some recommendations are made for future work to evaluate the performance of photocatalytic catalysts, to reduce the generation of harmful intermediates and to design new PCO reactors with integrated UV source and reaction surface.

1. Introduction

Indoor air pollutants impact human health, comfort and productivity. Volatile organic compounds (VOCs) are among the most abundant chemical pollutants in the indoor air that we breathe (WHO, 1989; USEPA, 1990). Some of these compounds are associated with sick building syndrome (SBS) including mucous membrane irritation, headache and fatigue (WHO, 1989; USEPA, 1990; Little et al., 1994; Meininghaus et al., 1999; Kim et al., 2001; Wang et al., 2007; Auvinen and Wirtanen, 2008); others are known carcinogens (e.g., formaldehyde, acrolein (OEHHA, 2007)). Millions of people are currently suffering from the consequences of poor indoor air quality and billons of dollars are lost in the world each year due to poor indoor air quality (Fisk and Rosenfeld, 1997). Many advanced technologies for the quick and economical removal of VOCs from indoor air have recently been developed. Among these, photocatalytic oxidation (PCO) is an innovative and promising approach (Tompkins, 2001).

As the pioneers in this field, Fujishima and Honda (1972) discovered the phenomenon of photoinduced water cleavage to TiO_2 electrodes. In the subsequent three decades, a wide range of potential applications of PCO to air purification have been reported. A literature search using the ISI Web of Knowledge database of articles published prior to March 2008 was carried out. The search keywords used were "photocatalytic oxidation" and "air or gas". The literature search identified 1906 articles. Of these, 1264 articles were excluded for one or more of the following reasons: (i) the studies performed were not on indoor air; (ii) they lacked data on VOCs, (iii) they were written in a language other than English. Consequently, 168 studies have been scrutinized for this paper.

The air purification technique of PCO commonly uses nano-semiconductor catalysts and ultraviolet (UV) light to convert organic compounds in indoor air into benign and odorless constituents – water vapor (H_2O) and carbon dioxide (CO_2) (Tompkins, 2001). Most PCO reactors use nano-titania (TiO_2) as the catalyst that is activated by UV light. Fig. 1 shows the schematic of the UV-PCO process of VOCs using TiO_2 as the catalyst. An electron in an electron-filled valence band (VB) is excited by photo-irradiation to a vacant conduction band (CB), leaving a positive hole in the VB. These electrons and positive holes drive reduction and oxidation, respectively, of compounds adsorbed on the surface of a photocatalyst (Ohtani, 2008).

The activation equation can be written as:

$$TiO_2 + h\nu \rightarrow h^+ + e^- \quad (1)$$

In this reaction, h^+ and e^- are powerful oxidizing and reducing agents, respectively. The oxidation and reduction reactions can be expressed as:

* Corresponding author. Fax: +86 10 6277 3461.
E-mail address: zhangyp@tsinghua.edu.cn (Y. Zhang).

1352-2310/$ – see front matter © 2009 Elsevier Ltd. All rights reserved.
doi:10.1016/j.atmosenv.2009.01.034

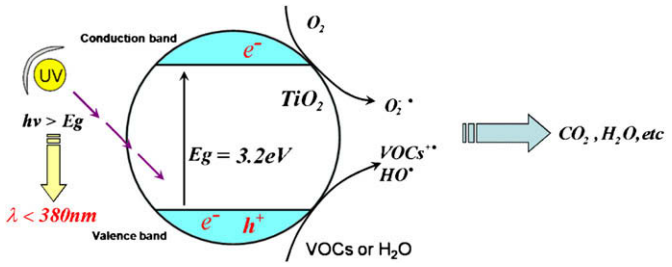

Fig. 1. Schematic of TiO_2 UV photocatalytic oxidation process of VOCs.

$$\text{Oxidation reaction}: h^+ + OH^- \rightarrow OH^\bullet \quad (2)$$

$$\text{Reduction reaction}: e^- + O_{2ads} \rightarrow O_{2ads}^- \quad (3)$$

When organic compounds are chemically transformed by a PCO device, it is the hydroxyl radical (OH•), derived from the oxidation of adsorbed water or adsorbed OH^-, that is the dominant strong oxidant. Its net reaction with a VOC can be expressed as:

$$OH^\bullet + VOC + O_2 \rightarrow nCO_2 + mH_2O \quad (4)$$

The process of PCO has several advantages (Ollis, 2000): (1) GRAS (Generally Recognized As Safe): the common photocatalyst is anatase TiO_2, an n-type semiconductor oxide which is also a component of some toothpastes and pharmaceutical suspensions; (2) Mild oxidant: Kinetic studies demonstrate that the ultimate source of oxygen during oxidation is molecular oxygen, a far milder oxidant than hydrogen peroxide or ozone, etc.; (3) Ambient temperature: photocatalysis appears to be active at room temperature; (4) general: while several mechanistic pathways for oxidation have been proposed, the dominant view is that the hydroxyl radical (or some other equally strong oxidant) is photogenerated on the titania surface; the potency of this oxidant is responsible for the titania's broad activity toward various contaminants (such as aromatics, alkanes, olefins, halogenated hydrocarbons, odor compounds etc.).

This paper is intended to provide a comprehensive review of the current understanding of PCO for indoor air purification, including photocatalysts, experiments, photocatalytic reactors, as well as the intermediates (see Fig. 2). This will be followed by a discussion of the kinetic models of the PCO process. Subsequently, the mechanism models of PCO reactors and the enhancement methods of PCO reactor performance are reviewed. The identification of PCO intermediates or by-products is summarized and discussed in the final section of this paper.

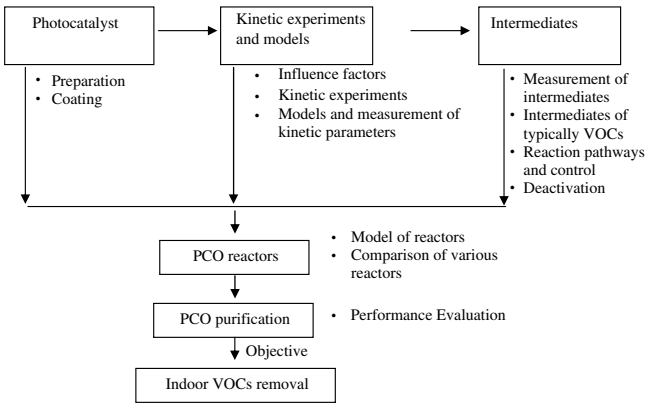

Fig. 2. Review frame of PCO.

2. Photocatalysts

Various catalysts have been developed for PCO applications. Table 1 summaries some of the photocatalysts described in the literature.

2.1. Common photocatalysts

The common photocatalysts are primarily metal oxides or sulphides, i.e., TiO_2, ZnO, ZrO_2, SnO_2, WO_3, CeO_2, Fe_2O_3, Al_2O_3, ZnS and CdS (Hoffmann et al., 1995). The most popular choices of photocatalysts are TiO_2 and ZnO. Teichner et al. (Ollis, 2000) explored the photoactivity of numerous oxides for hydrocarbon partial oxidation in the gas phase, finding that the active catalysts involving titania, zinc, and tungsten ranked in the activity sequence: TiO_2 (anatase) > ZnO > WO_3. Much of the published work on photocatalysis uses TiO_2 as it is relatively inexpensive, stable chemically, and the photogenerated holes are highly oxidizing (Fujishima and Zhang, 2006). TiO_2 has two crystal forms: anatase and rutile. The energy band-gaps of anatase and rutile are 3.23 and 3.02 eV, respectively. The commercial Degussa P25 prepared by flame pyrolysis (Maira et al., 2000) was used widely in air purification (Larson et al., 1995; Kirchnerova et al., 2005) with a primary particle diameter of 300 nm, a surface area of 50 $m^2\ g^{-1}$, and a crystal distribution of 70% anatase and 30% rutile (Larson et al., 1995). In addition, many researchers have attempted to improve the catalytic activity of photocatalysts by synthesizing semiconductor metal nanoparticle composites and to extend the photoresponse into the visible range by doping metal ions into TiO_2 (Ollis, 2000).

2.1.1. Visible light responsive photocatalyst

Usually, there are three ways to prepare the visible light responsive photocatalyst: doping TiO_2 with transition metal ions; doping nitrogen into TiO_2 and utilizing sensitizing dyes (Kamat and Meisel, 2002).

Coupling of TiO_2 with a small band-gap semiconductor or doping with transition metal ions such as V, Cr, Mn, Fe, Co, Ni, or Cu extends light absorption into the visible region (Zang et al., 2000). The coupling of low concentrations of WO_3 (4 wt.%) with mesoporous anatase TiO_2 led to high photocatalytic efficiency using both UV and visible light activation on toluene decomposition (Bosc et al., 2006). Furthermore, even though metal ion doping extended the response into visible light, the photocatalytic performance in the UV region decreased significantly (Kamat and Meisel, 2002). Brezova et al. (1997) found the presence of metals, such as Li^+, Zn^{2+}, Cd^{2+}, Ce^{3+}, Co^{3+}, Cr^{3+}, Fe^{3+}, Al^{3+}, Mn^{2+} and Pt°, may significantly change the photoactivity of TiO_2. He used the sol–gel technique to prepare the M^{n+}/TiO_2 layers for phenol degradation ($M^{n+} \equiv Li^+$, Zn^{2+}, Cd^{2+}, Ce^{3+}, Co^{3+}, Cr^{3+}, Fe^{3+}, Al^{3+}, Mn^{2+} and Pt^0). It was indicated that the presence of Co^{3+}, Cr^{3+}, Ce^{3+}, Mn^{2+}, Al^{3+} and Fe^{3+} ions in the TiO_2 photocatalyst (5 mol% M^{n+}:Ti^{4+}) has a detrimental effect on its photoactivity. A study of Uosaki et al. (Kamat and Meisel, 2002) has shown that inclusion of transition metal ions decreased photocatalytic activity of TiO_2 under UV irradiation. The metal ions act as recombination sites for the photogenerated charge carriers.

Various nitrogen-doped TiO_2 were found to photodegrade gaseous formaldehyde (Irokawa et al., 2006), acetaldehyde (Asahi et al., 2001; Irokawa et al., 2006), acetone (Ihara et al., 2003), 2-propanol (Irie et al., 2003; Miyauchi et al., 2004) and toluene (Irokawa et al., 2006; Wu et al., 2008). $TiO_{2-x}N_x$ (films and powders) has better photoactivity than TiO_2 under visible light irradiation. The active wavelength of $TiO_{2-x}N_x$, of less than 500 nm, covers the main peak of the solar irradiation energy beyond Earth's atmosphere (around 460 nm) (Asahi et al., 2001). Additional introduction of ZrO_2 into $TiO_{2-x}N_x$ displayed higher porosity, higher specific surface area, and an improved thermal stability than the

Table 1
Summary of various photocatalysts.

Catalyst composition	Preparation/coating method	Configuration	Compounds	Author, year
Commercial Deguss P25				
P25	Dip-coating	P	2-Propanol	Larson et al., 1995
			Formaldehyde, toluene	Obee, 1996
			Ethylene	Obee and Hay, 1997
			DCE	Wang et al., 1999
			Formaldehyde	Ao et al., 2004
			Formaldehyde	Mo et al., 2005
Other pure TiO_2 catalysts				
TiO_2	–	P	TCE, PCE	Hager and Bauer, 1999
	Sol–gel	F	DDVP	Yu et al., 2000
	Sol–gel	F	TCE	Maira et al., 2000
Visible light responsive photocatalyst				
$TiO_{2-x}N_x$	Sputtering	F	Acetaldehyde	Asahi et al., 2001
	Hydrothermal	F	Acetone	Ihara et al., 2003
	–	P	2-Propanol	Irie et al., 2003
	CVD	F	2-Propanol	Miyauchi et al., 2004
	–	–	Formaldehyde; acetaldehyde; acetone; benzaldehyde;	Irokawa et al., 2006
	APCVD	F	Rhodamine B	Guo et al., 2006
	MOCVD	P	Toluene	Li et al., 2007
M^{n+}/TiO_2	Sol–gel	F	Phenol	Brezova et al., 1997
Noble metal ions/TiO_2	Sol–gel	F	4-Chlorophenol	Zang et al., 2000
WO_x–TiO_2	Sol–gel and sintering	P	Methylene blue	Li et al., 2001
$TiO_{2-x}N_x/ZrO_2$	Sol–gel	F	Ethylene	Wang et al., 2006
WO_3–TiO_2	Sol–gel and dip-coating	F	Toluene	Bosc et al., 2006
Synthetical composites with metal				
Metal ion TiO_2	Sol–gel	P	CCl_4	Choi et al., 1994
Pd–TiO_2	Hydrothermal and sintering	P	Toluene	Belver et al., 2003
Ln^{3+}–TiO_2	Sol–gel	F	Benzene, toluene, ethylbenzene, o-xylene	Li et al., 2005
Synthetical composites with adsorption materials				
$TiO_2/SiO_2/ZrO_2$	Sol–gel	P	Ethylene	Fu et al., 1996a
TiO_2/SiO_2	Hydrothermal	P	Toluene	Mendez-Roman and Cardona-Martinez, 1998
Hybrid photocatalysts				
TiO_2 with ZnO, Al_2O_3, SiO_2, mordenite, and AC	–	P	Propionaldehyde	Yoneyama and Torimoto, 2000
Mesoporous (MCM-41), montmorillonite, β-zeolite	Sol–gel	P	Organic II	Bhattacharyya et al., 2004
TiO_2+AC	–	P	NO, NO_2, SO_2	Ao and Lee, 2004
ZnO + AC	Stirring	P	4-Acetylphenol	Sobana et al., 2008

P: powder; F: film; CVD: chemical vapor deposition; MPCVD: metal-organic CVD; APCVD: atmospheric pressure CVD; TCE: trichloroethylene; PCE: tetrachloroethylene; DCE: dichloroethylene; DDVP: dimethyl-2,2-dichlorovinyl phosphate; and AC: activated carbon.

unmodified $TiO_{2-x}N_x$ samples (Wang et al., 2006). Carbon is also used as a doping agent (Khan et al., 2002; Li et al., 2007). Khan et al. (2002) synthesized chemically modified n-type TiO_2 by the controlled combustion of Ti metal in a natural gas flame. This material, in which carbon substitutes for some of the lattice oxygen atoms, absorbs light at wavelengths below 535 nm and has lower band-gap energy than rutile (2.32 versus 3.00 eV).

Sensitizing dye is also used in the semiconductor with higher band-gap to change the electron-transfer processes during photocatalytic reaction. The principle of photosensitization of a semiconductor is illustrated by Vinodgopal et al. (1995). The energy difference between the oxidation potential of the excited sensitizer and the conduction band of the semiconductor acts as a driving force for the charge injection process. Charge injected from the excited dye molecule into the conduction band of TiO_2 can produce the dye cation radical (Nasr et al., 1996). Yet, it is necessary to regenerate the oxidized sensitizer with a suitable electron donor. Failure to regenerate the sensitizer will eventually cause its destruction (Vinodgopal et al., 1995).

2.1.2. Synthetic composites with metal and adsorption materials

A good photocatalyst depends strongly on the efficiency of electron–hole pair separation and the adsorption ability of gaseous VOCs.

To effectively eliminate the electron–hole recombination in the photocatalytic reaction, TiO_2 catalysts can be improved by doping some metal ions, coupling with other semiconductor oxides or depositing noble metals (Choi et al., 1994; Li et al., 2001; Zhang et al., 2006b). The presence of metal ion dopants in the TiO_2 crystalline matrix significantly influences photoreactivity, charge carrier recombination rates, and interfacial electron-transfer rates (Choi et al., 1994). Choi et al. (1994) found that doping with Fe^{3+}, MO^{5+}, RU^{3+}, OS^{3+}, Re^{5+}, V^{4+}, and Rh^{3+} at 0.1–0.5% significantly increased the photoreactivity for both oxidation and reduction, but Co^{3+} and Al^{3+} doping decreased the photoreactivity.

Another effect of doped metal is to decrease the deactivation of the photocatalysts. Belver et al. (2003) found that most of the Pd/TiO_2 catalysts showed a considerable increase in the conversion of toluene vapor under UV irradiation, while the benzaldehyde production decreased slightly compared with bare TiO_2. However, the main effect of palladium was to hinder the deactivation of the photocatalysts but not to enhance the photoactivity.

Binary catalysts with silica or ziroconia and TiO_2 were also shown to have significantly higher activities than pure titania for the complete photocatalytic oxidation of ethylene (Fu et al., 1996a). This may be due to TiO_2/SiO_2 and TiO_2/ZrO_2 having a higher surface acidity (Fu et al., 1996a; Mendez-Roman and Cardona-Martinez,

1998). However, isoelectric point measurements employing the sintered and unsintered catalysts showed no conclusive increase in surface acidity (Fu et al., 1996a). The mechanism of this promotion effect is not yet clearly understood. Mendez-Roman and Cardona-Martinez (1998) found the SiO_2–TiO_2 photocatalyst more active than TiO_2 and also that it deactivates at a slower rate. The binary oxide also seemed to have a higher toluene adsorption capacity than TiO_2. Some reports in the literature have shown that the incorporation of lanthanide ions such as La^{3+}, Eu^{3+}, Pr^{3+}, Nd^{3+}, and Sm^{3+} into the TiO_2 matrix could promote the chemical or physical adsorption of organic substrates on the catalyst's surface (Li et al., 2005).

2.1.3. Hybrid photocatalysts

According to chemical reaction kinetics (discussed in Section 3), the rate of chemical reactions is determined by the concentration of the chemical compounds (Yoneyama and Torimoto, 2000). However, TiO_2 exhibits low adsorption ability, especially for non-polar substances due to its polar structure (Bhattacharyya et al., 2004). The low adsorption ability of non-porous TiO_2 particles can be improved by making composites of TiO_2 with adsorbents. The adsorbents would absorb the compounds on the adsorbent support. Then a high concentration environment of the compounds was formed around the loaded TiO_2, resulting in an increase in the photoreaction rate. Yoneyama and Torimoto (2000) used various adsorbents, such as zeolum, alumina, silica, mordenite, ferrierite, and activated carbon, as the support of TiO_2 and showed that the hybrid photocatalysts were effective in achieving high decomposition rates of propionaldeyde in air. Similar results were obtained by Ao and Lee (2004), using activated carbon with TiO_2 as the hybrid photocatalysts. Not only TiO_2, but also ZnO was found to have higher photodegradation efficiency when synergized with activated carbon as the adsorbent (Sobana et al., 2008).

2.2. Preparation of photocatalysts

The methods for preparing nanometer TiO_2 can be summarized as follows: the sol–gel method (Livage, 1991; Yu et al., 2000), vapor decomposition of titanium alkyloxides (Rubio et al., 1997) or $TiCl_4$ in oxygen (Maira et al., 2000; Zeatoun and Feke, 2006), the hydrothermal technique (Cheng et al., 1995; Zheng et al., 2000; Guo et al., 2003), and water-in-oil microemulsion (Monnoyer et al., 1995; Qi et al., 1996). Based on the preparation conditions, methods used for the preparation of nanometer TiO_2 are divided into two types: gas-phase and liquid-phase methods.

2.2.1. Gas-phase methods

2.2.1.1. Gas-phase flame hydrolysis of $TiCl_4$. This gas-phase process includes fully mixing gasified $TiCl_4$ with reactant gases (hydrogen and oxygen). By burning the reactant gas at high temperature, the high temperature hydrolysis reaction will take place. The reaction is as follows:

$$TiCl_{4(g)} + 2H_{2(g)} + O_{2(g)} \rightarrow TiO_{2(s)} + 4HCl_{(g)} \quad (5)$$

The TiO_2 prepared by this gas-phase hydrolysis method is a complex oxide with coexisting anatase and rutile phases (Maira et al., 2000). It consists of 25–30 nm primary particles forming a loose aggregation measuring 140–170 nm. The commercial Degussa P25 is made using this method.

2.2.1.2. Gas-phase oxidation of $TiCl_4$. Titania powders can be produced by oxidizing volatile metal chlorides (e.g., $TiCl_4$) at high temperature using flame-aerosol reactors and near atmospheric pressure. The product is represented by the reaction below (Zeatoun and Feke, 2006):

$$TiCl_{4(g)} + O_{2(g)} \rightarrow TiO_{2(s)} + Cl_{2(g)} \quad (6)$$

2.2.1.3. Gas-phase hydrolysis of titanium alkoxides. The vapors of titanium alkoxides ($Ti(OR)_4$) and water are sprayed with nitrogen gas into a hydrolysis chamber. The hydrolysis reaction rapidly occurs to form spherical TiO_2 particles. The hydrolysis steps are:

$$Ti(OR)_{4(g)} + 4H_2O_{(g)} \rightarrow Ti(OH)_{4(s)} + 4ROH_{(g)} \quad (7)$$

$$Ti(OH)_{4(s)} \rightarrow TiO_2 \cdot H_2O_{(s)} + H_2O_{(g)} \quad (8)$$

$$TiO_2 \cdot H_2O_{(s)} \rightarrow TiO_{2(s)} + H_2O_{(g)} \quad (9)$$

Rubio et al. (1997) used the titanium alkoxide [$Ti(C_4H_9O)_4 \cdot C_4H_9OH$] to develop a type of spherical TiO_2 particle using this hydrolysis method.

2.2.2. Liquid-phase methods

2.2.2.1. Sol–gel method. The sol–gel method is recognized as an efficient method to prepare a porous TiO_2 coating from alkoxide solutions (Yu et al., 2000). Usually, the sol–gel process is also a hydrolysis process of titanium alkoxides, but it occurs in solution. It is based on the hydrolysis and condensation of molecular precursors. The chemical control of these reactions allows the formation of monodispersed powders, thin films, or fibers directly from the solution at low temperature (Livage, 1991). Wide application of titanium alkoxides as precursors in sol–gel synthesis led to extensive use of the hydrolysis reactions of $Ti(OR)_4$. The reaction scheme proposed by Livage is generally accepted and introduced clearly by Golubko et al. (2001).

2.2.2.2. Liquid-phase hydrolysis of $TiCl_4$. Titania can also be formed from a liquid-phase hydrolysis reaction, and this route has also been used commercially to manufacture TiO_2 into a fine particulate form (Zeatoun and Feke, 2006). $TiCl_4$ is soluble in cold water, and the hydrolysis reaction proceeds rapidly at mild temperatures. The overall reaction chemistry is:

$$TiCl_4 + 2H_2O \rightarrow TiO_2(\text{anatase}) + 4HCl \quad (10)$$

or

$$TiCl_4 + 2H_2O \rightarrow TiO_2(\text{rutile}) + 4HCl \quad (11)$$

The two reactions can occur in parallel, but the second one is more thermodynamically favorable (Zeatoun and Feke, 2006).

2.2.2.3. Hydrothermal. The hydrothermal method to prepare TiO_2 powder uses liquid solutions as solvents to produce the precursors under high temperature (in general $<250\ ^\circ C$ (Cheng et al., 1995)) and high-pressure conditions. With nucleation and crystal formation, crystalline products with different composition, structure, and morphology can be formed (Cheng et al., 1995). After being washed and dried, the TiO_2 powders are obtained. $TiCl_4$ and ($Ti(SO_4)_2$) were commonly used as the precursor (Cheng et al., 1995; Zheng et al., 2000), with a solution of NaOH (Zheng et al., 2000) or ethanol and water (Wu et al., 2007) commonly used as the solvents. The hydrothermal technique is widely employed to enhance crystallization for both laboratory and commercial scales. However, many factors such as reaction temperature, reaction time, type of precursor and the medium, may influence the crystallization process (Guo et al., 2003).

2.2.2.4. Water-in-oil microemulsion. The preparation of monodisperse nanoparticles using water-in-oil microemulsions is

a rapidly growing field (Monnoyer et al., 1995). The water-in-oil microemulsion is a thermodynamically stable, optically isotropic dispersion of surfactant stabilized microdrops of water in an external oil phase (Qi et al., 1996). The highly dispersed nanosize droplets are suited for particle synthesis and have the potential for controlling the microenvironment where chemical reactions may occur. However, the oil phase may pollute the surface of the resultant particles. A post-treatment has been developed to avoid adverse effects to the performance of catalysts.

2.3. Coating methods

The TiO_2 coating will also affect the photocatalytic activity. Some research has shown that TiO_2 film has a much higher photocatalytic activity than the most active commercial TiO_2 powder (Huang et al., 1999). There are two types of coating methods. The first one is to handle the catalyst powders by directly sintering (Cheng et al., 1995) or dip-coating (sometimes called wash-coating) (Obee and Brown, 1995; Mo et al., 2005). The other method is to form the TiO_2 film on the support, using chemical vapor deposition (CVD) (Yates et al., 2006), metal-organic CVD (MOCVD) (Guo et al., 2006; Zhang et al., 2006b; Li et al., 2007), sol–gel (Yu et al., 2000; Golubko et al., 2001) or spray coating (Drelich et al., 1998).

2.4. Deactivation

Photocatalyst lifetime is potentially important in process economics, as it sets maximum run times between catalyst regeneration or replacement (Sauer and Ollis, 1996a). Gas–solid photocatalyst activity has been observed to decrease with time (Ollis, 2000), which is due to the decrease of active (illuminated) catalyst sites on the reaction surface (Sauer and Ollis, 1996a).

There are several reasons for the loss of active catalyst sites. First, the generation of reaction residues (by-products or intermediates) may be adsorbed onto the catalyst and block the active sites, which as a result reduces the photocatalytic reaction (Ollis, 2000). This type of deactivation appears to be very common and includes reports for toluene (Blanco et al., 1996; D'hennezel et al., 1998), ethanol (Piera et al., 2002) and trichloroethylene, dimethylsulfide, and trichloropropene (Ollis, 2000). The detailed information about the deactivation caused by by-products or intermediates will be discussed in Section 5. Second, some species may photopolymerize on the surface, especially in the absence of water. Benzene conversion seems to provide such an example (Ollis, 2000). Third, species with heteroatoms such as N and S may undergo strong or complete photooxidation, leading to oxidized inorganic forms of nitrogen and sulphur which accumulate on the surface (Sauer and Ollis, 1996a). Finally, the fouling (i.e. particle materials) may change the catalyst surface by blocking pores (Zhao and Yang, 2003).

3. Kinetic experiments and models of PCO reaction rate

The photocatalytic reaction rate is important for evaluating the performance of photocatalytic VOC removal. It is also commonly used to calculate the reaction kinetic coefficients and the adsorption coefficients, the representative characteristic parameters of photocatalysts. Kinetic experiments were performed to study the influencing factors (such as temperature, humidity, light wavelength/intensity, oxygen concentration, contaminant concentration, surface velocity, resident time and catalyst loading) on the photocatalytic reaction rate. It is noted that not all the influencing factors were introduced clearly in some papers (see Table 2).

The kinetic models were also developed to describe the performance of various PCO reactors.

3.1. Experiments of influence factors in the PCO reaction process

3.1.1. Ultraviolet (UV) source and intensity

As the essential component to the PCO reaction process, the UV light (wavelength and intensity) has a great effect on the PCO reaction rate. Theoretically, the UV light with wavelength less than $<$380 nm could activate titania photocatalysts. Although some researchers developed a visible light responsive photocatalyst (Section 2), the germicidal lamp (UV-C, 254 nm) and fluorescent black-light lamp (300–370 nm) were more commonly used (Sauer and Ollis, 1996b; Obee and Hay, 1997; Benoit-Marquie et al., 2000; Attwood et al., 2003). It is reported that more intermediates were produced using a germicidal source than using a black-light source (please list the original paper rather than the review paper). In addition, an ultraviolet light-emitting diode (UV-LED), long-lasting, robust, small in size and high in efficiency, was also applied as the UV source during PCO oxidation (Chen et al., 2005). The commercial UV-LED used in PCO has a typical output of 12–20 mW (Chen et al., 2005; Shie et al., 2008). However, its peak wavelength is normally greater than 360 nm and requires a specific responsive photocatalyst for its application.

The reaction rate increased with increasing light intensity, as the heterogeneous photocatalytic reaction depends on the irradiation of TiO_2 surface by UV light to produce electron/hole pairs, even though part of them recombined (Wang et al., 1999). Egerton and King (1979) found that the influence of UV intensity on the reaction rate can be separated into two regimes: a first-order regime where the electron–hole pairs are consumed more rapidly by chemical reactions than by recombination, and a half-order regime where the recombination rate dominates. One sun equivalent was used to determine the regimes (Obee, 1996). The functional dependence of the PCO reaction rate, r, on UV light intensity is:

$$r = KI^n, (n = 1, \text{when} : I < S_\lambda; n = 0.5, \text{when} : I > S_\lambda) \quad (12)$$

where K is a constant, I is the UV intensity; S_λ is the one sun equivalent under the λ wavelength.

The one sun equivalent is about 1–2 mW cm^{-2} for wavelengths below 350 and 400 nm, respectively (Obee and Brown, 1995). This measured value agreed well with the results obtained by Jacoby et al. (1995), Obee (1996) and Wang et al. (1999).

Based on Eq. (12), the kinetic reaction rate r under the UV intensity, I, can be predicted by the following function (Hossain et al., 1999):

$$r = r_e \left(\frac{I}{I_e}\right)^n \quad (13)$$

where I_e is the UV intensity for which the kinetic reaction rate, r_e, has been evaluated.

The radiation fields inside the PCO reactors or devices have also been studied and simulated using various methods, such as view factors (Raupp et al., 1997; Hossain et al., 1999), Monte Carlo simulation (Changrani and Raupp, 1999) and empirical modeling (Wang and Ku, 2003) in order to get the optimal design for PCO reactors.

3.1.2. Pollutant concentration

The relationship between pollutant concentrations and reaction rate follows the Langmuir-Hinshelwood (L–H) model or the other power law models (see Section 3.2 for the details). This applies to many pollutants: acetone (Peral and Ollis, 1992; Sauer and Ollis, 1994), formaldehyde (Peral and Ollis, 1992; Obee and Brown, 1995; Yang et al., 2004), toluene (Obee, 1996) and trichloroethylene (TCE) (Hager and Bauer, 1999; Sanchez et al., 1999). Usually, there is an optimal pollutant concentration that will maximize the PCO reaction rate when the other conditions are stable.

Table 2
Experimental results of influence factors in PCO reaction process.

Author, year	VOCs	Deactivation	Influence factors of reaction rate								
			VOC conc. (ppm)	Oxygen conc. (%)	T (°C)	Humidity (ppm)	Resident time (s m^{-1})	Light			Catalyst loading (mg cm^{-2})
								Light source	Primary length (nm)	Intensity (mW cm^{-2})	
Alcohols											
Sauer and Ollis, 1996b	Ethanol	Y	47–209	–	27	14 400	3.0	MP Hg	200–300	–	0.002
Benoit-Marquie et al., 2000	1-Butanol	Y	292–1621	20	30	0	1818–515	MP Hg/ XeCl	300–380	–	–
Alkenes											
Obee and Hay, 1997	1–3 Butadiene	–	0.3–100	20	12.8–60	2000–20 000	11.11	HP Hg–Xe	250–350	9	2–3% by weight-manufacturer's claim
Obee and Hay, 1997	Ethylene	–	1–1000	15	2–48	0–100	0.75	BL	352	5.6	0.74
Fu et al., 1996b	Ethylene	–	140	21	107	–	–	–	365	–	–
Aldehydes											
Obee and Brown, 1995	Formaldehyde	–	0.5–100	20	12.8–60	2000–20 000	83.33	HP Hg–Xe	250–350	9	2–3% by weight-manufacturer's claim
Sauer and Ollis, 1996b	Acetaldehyde	Y	16.4–180	–	27	14 400	3.0	MP Hg	200–300	–	0.002
Sano et al., 2004	Acetaldehyde	Y	100	–	40–190	38 000	27.5	BL	–	5.0	1.0
Ketones											
Zorn et al., 1999	Acetone	Y	143–1652	–	30–113	>21 500	151–708	BL	365–370	2.3–3.1	–
Attwood et al., 2003	Acetone	Y	11 738	9	25	0	–	Hg-Xe	>250	–	–
Aromatics											
Obee and Brown, 1995	Toluene	–	0.29–20	20	12.8–60	2000–20 000	83.33	HP Hg–Xe	250–350	33	2–3% by weight-manufacturer's claim
Sano et al., 2004	Toluene	Y	15	–	40–190	62 500	135	BL	–	5.0	1.0
Others											
Sanchez et al., 1999	TCE	Y	30–184	–	60–250	–	11.8–782.6	Xe	340	–	–
Hager and Bauer, 1999	TCE	Y	91.6–17 000	–	20–70	0–382	64.7–107	MP Hg	365	32.6	–

T: temperature; TCE: trichloroethylene; PCE: tetrachloroethylene; HP Hg–Xe: high-pressure Hg–Xe lamp; BL: black light; MP Hg: medium pressure mercury lamp, XeCl: xenon-chloride excimer lamp.

It is noted that the pollutant concentrations used in the models should be the concentrations on the reaction surface but not the inlet ones. For a real PCO reaction process, they may be very different because of the limited (convective) mass transfer (Yang et al., 2007). The method for obtaining the concentration on the reaction surface will be introduced at Section 3.3.

3.1.3. Humidity

The molecular water adsorbed on the photocatalyst will react with the hole and generate some hydroxyl groups, such as OH• (Fig. 1), which, in turn, oxidizes pollutants. It has been found that a PCO reaction is typically governed by the generation of the hydroxyl radical (Park et al., 1999; Tompkins, 2001), although reactions that generate other radicals (e.g., chlorine (Yamazaki et al., 1996)) can display higher reaction rates. In the absence of water vapor, the photocatalytic degradation of some chemical compounds (e.g., formaldehyde (Ao et al., 2004), acetone (Chang et al., 2003), toluene (Luo and Ollis, 1996; Kim and Hong, 2002)) is seriously retarded. However, excessive water vapor on the catalyst surface will inhibit the reaction rate because the presence of water vapor competes with pollutants for adsorption sites on the photocatalyst, thus reducing the pollutant removal rate (Obee and Hay, 1997). This is called "competitive adsorption" between water vapor and pollutant. The inhibiting effect of water on the PCO reaction rate was also reported in the literature, including formaldehyde (Ao et al., 2004), acetone (Chang et al., 2003), toluene (Luo and Ollis, 1996), ketone (Raillard et al., 2004), m-xylene (Peral and Ollis, 1992), TCE (Wang et al., 1998) etc.

In addition, the relationship between water vapor concentration and PCO reaction rate was quantitatively analyzed. Some studies summarized the experimental data with empirical equations. For instance, Peral and Ollis (1992) found the rate of acetone oxidation decreased with increasing water vapor. The empirical expression developed is as follows:

$$r = \frac{r_0}{1 + K_H C_w^{\beta}} \tag{14}$$

where r_0 is the PCO reaction rate with no water vapor present ($r_0 = 0.909$ μg (min cm^2)$^{-1}$), C_w is the concentration of water vapor (mg m^{-3}), K_H and β are two constants fitted by the experimental data ($K_H = 9.6 \times 10^{-7}$ m^3 mg^{-1} and $\beta = 17$).

The bimolecular Langmuir–Hinshelwood (BLH) model was commonly used to study the influence of water vapor on reaction rate. Obee et al. (Obee and Brown, 1995; Obee, 1996; Obee and Hay, 1997) studied the effect of moisture on the PCO reaction rate of formaldehyde, ethylene, toluene, and 1–3 butadiene. All of them followed the BLH model. Theoretically, there should be an optimal concentration of water vapor to get the maximal PCO reaction rate. This was proved by the other experimental results (Luo and Ollis, 1996; Nam et al., 2002; Chang et al., 2003).

The presence of water vapor also affects the generation of PCO intermediates or by-products. For example, the conversion of formaldehyde and the yield of its by-product, formic acid, decreases with increasing humidity levels (Ao and Lee, 2004).

3.1.4. Temperature

Temperature not only affects the PCO kinetic reaction but also the adsorption of the gas-phase compounds on the photocatalyst. The reaction kinetic coefficient, k, followed an Arrhenius temperature dependence formula (Obee and Hay, 1997):

$$k \propto f\left(\exp\left(\frac{-E}{RT}\right)\right) \tag{15}$$

where E is an apparent activation energy, normally greater than nil; T the titania temperature and R the gas constant (1.99×10^{-3} kcal (mol K)$^{-1}$). Hence, increasing temperature positively affects the PCO kinetic reaction.

During an adsorption process, the coverage of photocatalyst surfaces by the pollutants decreases progressively with increasing temperature (Serpone and Pelizzetti, 1989). The adsorption equilibrium coefficient, K, also followed a temperature-dependent equation, similar to the Arrhenius one:

$$K \propto f\left(\exp\left(\frac{-H}{RT}\right)/\sqrt{T}\right) \tag{16}$$

where H is the change in enthalpy accompanying adsorption for the adsorbed pollutant.

The total PCO reaction rate is the combined process of kinetic reaction and adsorption (see Section 3.2 for the details). With increasing temperature, the PCO reaction rate will increase and then drop. A maximal PCO reaction rate should appear at an optimal temperature (Serpone and Pelizzetti, 1989).

The phenomenon described here was also investigated for different VOC compounds under various temperature conditions. Acetaldehyde (Sano et al., 2004), toluene (Obee and Brown, 1995), butadiene (Obee and Brown, 1995), trichloroethylene (TCE) (Hager and Bauer, 1999; Sanchez et al., 1999) and perchloroethylene (PCE) (Hager and Bauer, 1999) were found to have decreasing reaction rates with increasing temperatures (Table 2). However, for the compounds of ethylene (Fu et al., 1996b; Obee and Hay, 1997) and formaldehyde (Obee and Brown, 1995), the reaction rates increased with increasing temperatures (Table 2). This may be ascribed to the relatively limited ability of reaction and adsorption (mass transfer). Under the reaction limit process, the increasing temperature will enhance the reaction rate and the negative effect on adsorption becomes negligible. Whereas, the increasing temperature decreases the amount of adsorbed pollutants on the reaction surface so that it lowers the reaction rate under the mass transfer limit process.

In addition, the optimal temperature seems to be in a narrow range (Serpone and Pelizzetti, 1989). Zorn et al. (1999) found that increasing the reaction temperature from 30 to 77 °C (in a dry feed stream) increased the reaction rate constant of vapor acetone at a 95% confidence level; however, increasing the temperature from 77 to 113 °C did not have a significant effect.

3.1.5. Others

3.1.5.1. Oxygen. The presence of oxygen is essential for the photoreaction to occur (Augugliaro et al., 1999). Usually, the pollutant decomposition rate increased with increasing oxygen concentration (Augugliaro et al., 1999; Chang et al., 2003) although the competitive adsorption effect between oxygen and pollutants seems not strong. Furthermore, abundant oxygen will promote the PCO reaction to completion. Yamazaki et al. (1996) found that the by-product formation of trichloroethylene (TCE) was reduced by increasing oxygen concentration in the feed gas stream.

3.1.5.2. Inhibitive and promotive effect of mixture. Due to the competition of adsorption and photon-irradiation among multi-compounds, the PCO reaction rate should be commonly inhibited. Chen and Zhang (2008) found in the 16 VOC mixture test on toluene, ethylbenzene, octane, decane and dodecane etc., that the inhibited effect among different VOCs became quite obvious. However, if the additional compounds are decomposed into radicals with high oxidation performance, e.g., chlorine (Yamazaki et al., 1996), the reaction rate may be enhanced.

3.1.5.3. Cl radicals. Some chlorocarbon compounds with molecular chlorine, such as trichloroethylene (TCE), 1,1,3-trichloropropene (TCP) and perchloroethylene (PCE) have higher photoefficiency than toluene, benzene etc.

In the case of photocatalytic oxidation of TCE and toluene mixtures in air, the Cl radicals, Cl•, activate toluene by chain transfer (Eq. (17)) and thus dramatically increase the toluene rate of conversion (Luo and Ollis, 1996).

$$Cl^{\bullet} + C_6H_5CH_3 \rightarrow C_6H_5CH_2^{\bullet} + HCl \tag{17}$$

With the addition of TCE, it was demonstrated that destruction of toluene could raise the toluene photoefficiency to provide 100% conversion in a single pass with a residence time of about 5–6 ms (D'hennezel and Ollis, 1997). Sauer et al. (1995) obtained a similar promotion of TCP and PCE to the toluene PCO oxidation rate. It is interesting that a chloride compound was promoted by the presence of an organic compound. It was observed that the presence of methanol as an electron donor resulted in higher degradation rates of carbon tetrachloride (CCl_4) (Alberici and Jardim, 1997).

3.1.5.4. Nitrogen monoxide (NO) and sulphur dioxide (SO_2). As common indoor air pollutants, the effects of NO and SO_2 on indoor organic pollutants (such as formaldehyde) were identified. The presence of NO promoted the conversion of indoor pollutants. The positive effect of NO is due to the hydroxyl radicals generated from the photodegration of NO as shown in the following reaction (Ao et al., 2004):

$$NO + HO_2^{\bullet} \rightarrow NO_2 + OH^{\bullet} \tag{18}$$

For SO_2, a sulfate ion was formed after the introduction of SO_2 gas (Ao et al., 2004). However, the sulfate ion competed with pollutants for adsorption sites on the photocatalyst surface. Thus, the presence of SO_2 inhibited the simultaneous conversions of all present pollutants, such as formaldehyde, ethanol (Ao et al., 2004), ethylene (Yamazaki et al., 2001), and dichloroethane (Chen et al., 1997).

3.2. Kinetic models of PCO reaction

PCO is a typical bimolecular reaction between surface oxygen (or an oxygen-containing molecule) and the reducible reactants (Serpone and Pelizzetti, 1989). For heterogeneous photocatalysis on TiO_2, the reaction rate can be obtained by considering the detailed mechanistic steps given by Hoffmann et al. (1995). In general, the PCO reaction rates can also be treated empirically as the decreasing rate of any reactants or the increasing rate of any product (Hoffmann et al., 1995). In the case of the PCO of a unimolecular reactant, R on TiO_2, the reaction occurs according to the following stoichiometry:

$$R + O_2 \xrightarrow{TiO_2,hv} A + B \quad (19)$$

where A and B are the reactants. The rate of R degradation is:

$$r = -\frac{d[R]}{dt} = -\frac{d[O_2]}{dt} = \frac{d[A]}{dt} = \frac{d[B]}{dt} \quad (20)$$

A common way to express the reaction rate is to use the power law:

$$r = -\frac{d[R]}{dt} = k[R]^n \quad (21)$$

where $[R]$ is the concentration of R, k is the rate constant and n is the order of the reaction, n is equal to 0 (Jacoby et al., 1995; Choung et al., 2001), 1 (Zhang et al., 2003) etc.

However, it is impossible to find the dependence of the reaction rate on the influencing factors mentioned in Section 3.1. Kinetic models including the influencing factors need to be developed. Because the reactions always involve adsorption steps before electron exchange, the adsorption isotherms are expected to play an important role in the reported kinetic models. The rate equations derived from isotherms or rate constants are as follows (Serpone and Pelizzetti, 1989; Peral et al., 1997):

a) The Mars-Van Krevelen (MVK) mechanism, which involves the oxidation–reduction of the surface of the photocatalyst. The solid behaves as an intermediates reactant. Its surface oxygen anions are the oxidizing species, which are regenerated by gaseous oxygen.
b) The stationary-state adsorption (SSA) model, which is based on the oxidation–reduction of the adsorbed phase.
c) The Eley-Rideal (ER) mechanism, which involves the reaction between adsorbed oxygen and the gaseous reactant. For all the pollutant concentration (or partial pressure), the reaction rate remains of the first order with respect to the reactant.
d) The Langmuir–Hinshelwood (L–H) mechanism, which includes the reaction occurring between both reactants at their equilibrium of adsorption.

The L–H mechanism has been widely used to formulate the rate equations for the PCO reaction, that is, the reaction r is in proportion to the coverage of the reactants:

$$r = k\theta_R\theta_{O_2,ads} \quad (22)$$

where k is the reaction constant (dependent on T and UV intensity, etc.), θ_R represents the fractional coverage of R adsorbed to the photocatalyst surface and $\theta_{O_2,ads}$ represents the corresponding fraction of oxygen adsorbed to the surface.

Based on the Langmuir model for monolayer adsorption, the fractional coverage of R is defined as (Ruthven, 1984; Serpone and Pelizzetti, 1989):

$$\theta_R = \frac{q}{q_S} = \frac{m}{m_{max}} = \frac{K[R]}{1 + K[R]} \quad (23)$$

where q_S is the total number of adsorption sites per unit weight or volume of the photocatalyst (adsorbent), q is the number of adsorbed sites per unit weight or volume of the photocatalyst, m is the amount adsorbed per unit weight or volume of the photocatalyst, m_{max} is the maximum amount adsorbed, and K is the adsorption equilibrium coefficient.

An analogous expression can also be written for oxygen. Hoffmann et al. (1995) summarized the adsorption equilibrium coefficient of oxygen binding to Degussa P25 TiO_2 and found that it was in the range of 3.4×10^3 to 20×10^4 M^{-1} ($1\ M^{-1}$ is about $1\ mol\ L^{-1}$).

Considering the abundant oxygen in the atmosphere (about 20.8% by volume), the fractional coverage $\theta_{O_2,ads}$ is usually close to 1. Thus, Eq. (22) is usually written as the unimolecular type L–H model (ULH) (Peral and Ollis, 1992; Sauer and Ollis, 1994; Biard et al., 2007; Shiraishi et al., 2007; Yang et al., 2007):

$$r = k\theta_R = k\frac{K[R]}{1 + K[R]} \quad (24)$$

Eq. (24) has been used in many practical studies (Table 4).

Notice that Eq. (24) is only for the degradation and adsorption of a single compound. By considering the inhibiting effects (e.g., competitive adsorption) of multi-compounds (Lewandowski and Ollis, 2003a,b) and/or water vapor, and the effect of temperature, the ULH model has been improved by several types of formulas (see Table 3). Moreover, another corrected L–H equation with two different adsorption sites was developed by Vorontsov et al. (1999) and Coronado et al. (2003). The corrected equation was found to fit his experimental results very well, but still needs to be validated.

Considering that the water vapor is also one of the reactants during the PCO reaction (Fig. 1), the bimolecular L–H (BLH) model is applied as:

$$r = k\theta_R\theta_{water} \quad (25)$$

The BLH model was used to study the effects of humidity on the oxidation rates of formaldehyde, toluene and 1–3 butadiene by Obee and Brown (1995) (Table 3). In that case, the BLH model was found to provide a better correlation with the oxidation rate data than the ULH model.

There was however also some experimental evidence showing that the PCO process did not always follow an L–H model due to a fouling of the catalyst (Doucet et al., 2006).

3.3. Measurement method of kinetic parameters

The most common method evaluating the kinetic parameters is to choose one of the kinetic models (Table 3) and to put the measured kinetic data through a curve-fitting routine (a least-square optimization) (Zhao and Yang, 2003). The reaction rate, r and pollutant concentration, C are usually used as the necessary kinetic data for data fitting. Many researchers have obtained these kinetic parameters for different reaction models. Table 4 lists some results from the ULH model (Jacoby et al., 1995; Alberici and Jardim, 1997; Noguchi and Fujishima, 1998; Obuchi et al., 1999; Zorn et al., 1999; Bouzaza et al., 2006; Biard et al., 2007; Yang et al., 2007; Zhang et al., 2007). However, the results may not be comparable for two reasons. Firstly, the reaction conditions reported in the literature were very different (see Table 4), and most of them were out of the range of normal indoor air conditions. Secondly, most of the researchers handled the experimental data with different units (see Table 4), and some of these units were significantly wrong, such as $\mu mol\ L^{-1}$ used for the adsorption equilibrium coefficient, K.

In principle, the pollutant concentration, C should be the gas-phase concentration adjacent to the reaction surface, C_{surf}. This is difficult to measure directly with instruments. The concentration of pollutants in the air stream, C_{stream} is usually used in place of C_{surf} for data fitting purposes, which sometimes causes obvious errors in the kinetic parameter evaluation (Yang et al., 2007). The traditional way is to increase the airflow rate to enhance the convective mass transfer rate in order to reduce the difference between C_{stream} and C_{surf} (Obee, 1996; Obee and Hay, 1997). However, it is difficult to realize such conditions when PCO decomposes some pollutants under strong UV radiation, or decomposes multi-compounds simultaneously (Yang et al., 2007).

Table 3
Kinetic mechanism of PCO reaction.

Mechanism	Kinetic equation		Ref.
Power law	$r_A = kC_A^n$	½ order, $n = 0.5$	Zorn et al., 1999
		Zero order, $n = 0$	Jacoby et al., 1995; Choung et al., 2001
		First order, $n = 1$	Zhang et al., 2003; Liu et al., 2005; Zhang et al., 2006a
		Second order, $n = 2$	Zhao and Yang, 2003
ULH	$r_A = k\frac{K_A C_A}{1 + K_A C_A}$		Peral and Ollis, 1992; Sauer and Ollis, 1994; Biard et al., 2007; Shiraishi et al., 2007; Yang et al., 2007
ULH + MC	$r_A = k\frac{K_A C_A}{1 + K_A C_A + \sum_i K_i C_i}$		Wang et al., 1999; Lewandowski and Ollis, 2003a,b; Chen and Zhang, 2008
ULH + W + T	$r_A = \frac{k\exp(-E/RT)K_A\frac{\exp(-\Delta H_A/RT)}{\sqrt{T}}C_A}{1 + K_A\frac{\exp(-\Delta H_A/RT)}{\sqrt{T}}C_A + K_W\frac{\exp(-\Delta H_W/RT)}{\sqrt{T}}C_W}$		Obee and Hay, 1997
BLH	$r_A = k\frac{K_{A1}C_A}{1 + K_{A1}C_A + K_{W1}C_W}\frac{K_{A4}C_W}{1 + K_{A2}C_A + K_{W2}C_W}$		Obee and Brown, 1995; Yu et al., 2006; Chen and Zhang, 2008
	$r_A = k\frac{K_{A1}C_A}{1 + K_{A1}C_A}\frac{K_{A4}C_W}{1 + K_{W2}C_W}$		Vorontsov et al., 1999; Coronado et al., 2003

Mechanism: ULH: Unimolecular Langmuir–Hinshelwood; BLH: Biomolecular Langmuir–Hinshelwood; +W: with water competitive adsorption; +T: Temperature-dependent; +MC: with the inhibiting effect of multi-compounds. *Symbol description*: r: reaction rate; k: reaction rate constant; K: adsorption coefficient; C: concentration; E: apparent activation energy; ΔH: change in enthalpy; R: gas constant; T: temperature (K). *Subscripts*: A: decomposed pollutant; W: water vapor; i: multi-compounds.

Yang et al. (2007) developed a Mass Transfer Based (MTB) method for accurately obtaining the kinetic coefficients of various kinetic models. It takes the convective mass transfer effect into consideration by applying the simulated method to calculate the pollutant concentration, C_{surf}. The kinetic coefficients can then be regressed by using the measured reaction rates, r, and the calculated concentrations, C_{surf}. The relative measurement error of the MTB method was lower by about 75% than that of the conventional method in the cases published by Yang et al. (2007).

In principle, the adsorption coefficients K in Eq. (24) can be obtained independently from the dark adsorption isotherms of the photocatalyst. However, some researchers found that the coefficient K obtained in this way was different from the equivalent constant determined from kinetic data obtained in the photocatalytic kinetic experiment (Sauer and Ollis, 1996b; Zhao and Yang, 2003; Yu et al., 2006). This difference may be due to the following reasons. Firstly, the effect of temperature on the adsorption coefficient K is not fully considered. Some studies evaluated the adsorption coefficients under the same ambient or environmental temperature through PCO or dark adsorption kinetic data fitting. However, the temperature on the reaction surface is higher than that of dark adsorption conditions because of the UV irradiation (and even the heat release of adsorption/desorption). Based on the discussion in Section 3.1.1, temperature has a significant positive or inhibiting effect on the kinetic experiment. Thus, the comparison of K obtained by these two methods under the same environmental temperature is not reasonable. Secondly, it may be due to the different kinetic models chosen for the data fitting (Sauer and Ollis, 1996b). Thirdly, a PCO process includes various elementary steps (Sauer and Ollis, 1996b; Muggli et al., 1998). The data fitting of the kinetic experimental results only describes the equivalent adsorption effect. With different reaction conditions, the elementary steps and the products will be changed, which result in various adsorption parameters.

4. Intermediates

PCO reactions of VOCs proceed in a stepwise fashion, that is, they take more than one elementary step to complete. An

Table 4
Kinetic parameters of unimolecular Langmuir–Hinshelwood model of various pollutants.

Pollutants	Photocatalyst	VOC conc. (ppm)	PW (nm)/I (mW cm^{-2})	T (°C)/ RH (%)	Kinetic parameters		Ref.
Formaldehyde	STS-21 sol	30–2000	365/1.0	20/40	0.19 μmol min^{-1}	0.51 μmol L^{-1}	Noguchi and Fujishima, 1998
	P25	1.8	254/0.083	24/47	1.48 μmol (m^2 s)$^{-1}$	0.94 ppmv^{-1}	Yang et al., 2007
Acetaldehyde	STS-21 sol	30–2000	365/1.0	20/40	0.16 μmol min^{-1}	0.21 μmol L^{-1}	Noguchi and Fujishima, 1998
	TiO_2/SiO_2	3000–6200	300–400/–	67/–	3.89×10^{-4} L (g min)$^{-1}$	21.9 L mol^{-1}	Obuchi et al., 1999
	Pt–TiO_2/SiO_2	3000–6200	300–400/–	67/–	5.97×10^{-4} L (g min)$^{-1}$	36.9 L mol^{-1}	Obuchi et al., 1999
Acetone	P25	590	365/–	50/23	14.68 g (m^3 min)$^{-1}$	0.35 m^3 g^{-1}	Alberici and Jardim, 1997
	TiO_2/ZrO_2	143–1652	365/2.3–3.1	30/0	0.097 μmol ($L_{cat:rings}$ s)$^{-1}$	0.51 L μmol^{-1}	Zorn et al., 1999
Benzene	TiO_2/Sr_2CeO_4	117–308	254/–	39–60/–	0.0064 mg L^{-1}	9.2078 L mg^{-1}	Zhong et al., 2007
	P25	0.56–1.3	254/0.56	25–27/40	1.56 mol (m^2 s)$^{-1}$	0.77 m^3 mg^{-1}	Zhang et al., 2007
Toluene	P25	5.2–26	254/–	20/45–50	13.388 mg (m^3 s)$^{-1}$	0.0049 m^3 mg^{-1}	Bouzaza et al., 2006
	P25	1.2–7.2	254/0.56	25–27/40	6.77 mol (m^2 s)$^{-1}$	0.24 m^3 mg^{-1}	Zhang et al., 2007
TCE	P25	50 mTorr	356/5.3	20.8/2.69	101 μmol (m^2 s)$^{-1}$	0.022 m Torr^{-1}	Jacoby et al., 1995
	P25	538	365/–	50/23	28.05 g (m^3 min)$^{-1}$	0.21 m^3 g^{-1}	Alberici and Jardim, 1997
	P25	3.7–18.5	254/–	20/45-50	729.254 mg (m^3 s)$^{-1}$	0.0017 m^3 mg^{-1}	Bouzaza et al., 2006
Butane	P25	8.7–41.4	254/–	20/45–50	27.461 mg (m^3 s)$^{-1}$	0.0199 m^3 mg^{-1}	Bouzaza et al., 2006
Propionic acid	TiO_2 Millenium PC500	–	365/4	30/50	2.02–2.10 mmol (m^3 s)$^{-1}$	0.41–0.32 m^3 mmol^{-1}	Biard et al., 2007
Butyric acid	TiO_2 Millenium PC500	–	365/4	30/50	1.98–2.25 mmol (m^3 s)$^{-1}$	0.39–0.24 m^3 mmol^{-1}	Biard et al., 2007

I: Intensity; PW: primary wavelength.

intermediate is the reaction product of each of these steps, except for the last one, which forms the final product. In some published articles, these intermediates are also called "by-products". Actually, a by-product means the secondary or incidental product deriving from the PCO reaction that is not the primary product. In this paper, the word "intermediate" will be uniformly used.

Recent studies (e.g., Sun et al., 2008) have found that the reactions achieved by the PCO processes are not as complete as they had been assumed to be. Rather than oxidizing a given organic pollutant all the way to CO_2 and H_2O, the oxidation process sometimes stops along the way, yielding aldehydes, ketones or organic acids. Such unintended intermediates can be toxic or irritating and may be less acceptable for human health and comfort than their precursors. In such a setting, the PCO process becomes another source of pollutants. Furthermore, the generation of intermediates is one of the main causes of photocatalyst deactivation.

4.1. Analytic methods for intermediate identification

Gas chromatograph/flame ionization detector (GC/FID), gas chromatography/mass spectroscopy (GC/MS), high performance liquid chromatography (HPLC), Fourier-transform infrared spectroscopy (FTIR), temperature-programmed oxidation (TPO) and temperature-programmed hydrogenation (TPH) are often used to characterize the intermediates of a PCO reaction (Blanco et al., 1996; Luo and Ollis, 1996; D'hennezel et al., 1998; Augugliaro et al., 1999; Martra et al., 1999; Blount and Falconer, 2001, 2002; Marci et al., 2003; Irokawa et al., 2006). It appears that no significant intermediates were identified using GC/FID (Luo and Ollis, 1996). Combined with GC/FID/MS, GC/MS/HPLC, GC/FTIR or TPH and TPO, some intermediates were found on the reaction surface during the PCO processes. These were primarily solid-phase products, the only gas-phase intermediate found was CO. FTIR has been widely used to analyse the surface intermediates of PCO. However it seems that FTIR is only suited to situations where the pollutant concentration is high, from 30 to 13 000 ppm (Mendez-Roman and Cardona-Martinez, 1998; Augugliaro et al., 1999; Martra et al., 1999; Maira et al., 2001). Blount and Falconer (2001, 2002) studied the toluene intermediates at approximately 100 ppm using the TPH and TPO methods, and identified only benzaldehyde as the significant intermediate in their research. Applying HPLC (D'hennezel et al., 1998) or diffuse reflectance Fourier-transform infrared spectroscopy (DRIFTS) (Irokawa et al., 2006), the intermediates with concentrations of their parent pollutants of about 10–20 ppm were also identified. In order to detect the intermediates at such low levels, liquid nitrogen trapping (Ye et al., 2006) and adsorbent tube were usually used to concentrate these intermediates.

Real-time monitoring of pollutants is also very important for the study of PCO reactions, particularly to show temporal pollutant/intermediates and their continuous concentration variations (Grinshpun et al., 2005). Some real-time monitors for VOCs and their PCO intermediates are available. Photoacoustic Spectroscopy (PAS) and Proton Transfer Reaction Mass Spectrometer (PTR-MS) are two popular choices for real-time monitoring of VOCs at low concentrations. Photoacoustic Spectroscopy (PAS) is a kind of infrared spectroscopy which uses a microphone as the transducer. Obee et al. (Obee and Brown, 1995; Obee, 1996; Obee and Hay, 1997) and Zhang et al. (Zhang et al., 2003; Yang et al., 2004) used the typical set-up of photoacoustic systems (Brüel & Kjær or Innova Air Tech., Denmark) for monitoring the VOC decomposition by PCO. However, carbon monoxide was the only reported intermediate. The PTR-MS system can detect a larger range of organic compounds with molecular mass of 21–500 than a PAS system. PTR-MS is a chemical ionization technique based on proton-transfer reactions from H_3O^+ ions to gaseous organic analytes with a higher proton affinity than water (Wisthaler et al., 2007). It was expected to measure individual VOCs at 10 s with concentrations as low as a few pptv (parts per trillion by volume) (Hansel et al., 1998).

4.2. Intermediates of typical indoor VOCs generated by PCO

VOCs typically detected in indoor air belong primarily to several groups of compounds, such as aldehydes, ketones, alcohols (or alkoxyalcohols) and aromatics.

4.2.1. Alcohols, alkoxyalcohols

Methanol is the primary compound emitting from forest products that are widely used in modern buildings (Stokke et al., 2006). It is also a human bioeffluent (Wisthaler et al., 2007). Yang et al. (1996) found formaldehyde, methylal (formaldehyde dimethyl acetal) and methyl formate to be the main intermediates in the liquid-phase reaction of methanol. However, only formaldehyde was identified as the intermediate of methanol in the gas phase by Stokke et al. (2006).

Ethanol was photooxidized to acetaldehyde, formaldehyde and corresponding acids (Sauer and Ollis, 1996b; Vorontsov et al., 1997; Vorontsov and Dubovitskaya, 2004). Sauer and Ollis (1996b) proposed that ethanol reacted to form acetaldehyde, which then formed CO_2 through a formaldehyde intermediate. Furthermore, acetic acid and formic acid were also thought to be the intermediates if considering the completion of a transient carbon balance during ethanol degradation. However, Sauer did not directly identify these two acids. Applying TPO and TPD analysis methods, Muggli et al. (1998) identified acetaldehyde, acetic acid, formaldehyde and formic acid as the intermediates for the room temperature PCO of ethanol on TiO_2. The reactants and intermediates were labeled with ^{13}C in order to study the reaction pathway of each carbon. Thus, an ethanol photocatalytical degradation kinetic pathway was developed by Muggli et al. (1998). PTR-MS assessment of the intermediates of ethanol photocatalytical degradation was performed in a simulated aircraft cabin by Wisthaler et al. (2007). They found methanol was another incomplete PCO product of ethanol in addition to acetaldehyde and formaldehyde. However, no further discussion about the kinetic pathway of methanol generation was reported.

1-Butanol (or n-butanol, normal butanol) is primarily used as a solvent in indoor decoration. Six major intermediates, butanal (or butyraldehyde), butanoic acid, 1-propanol, propanal (or propionaldehyde), ethanol and acetaldehyde were identified in the case of the photocatalytic degradation of 1-butanol (Benoit-Marquie et al., 2000). Butanal was verified to be the first of 1-butanol by Benoit-Marquie et al. (2000), which agreed with the experimental result of Peral and Ollis (1992). Fig. 3 describes the mechanistic scheme of the photocatalytic oxidation of 1-butanol. An exhaustive reaction pathway as that shown by Muggli et al. (1998) leads to the formation of ethanol and acetaldehyde by the successive oxidation of 1-propanol, propionaldehyde and propanoic acid. Further degradation would yield methanol, formaldehyde and formic acid.

From the identified intermediates of the three alkoxyalcohols discussed above, it can be inferred that the alkoxyalcohols react through the pathway: alcohols → aldehydes → acids → shorter carbon-chain aldehydes + alcohols. The newly generated shorter carbon-chain aldehydes and alcohols will follow similar pathways to form methanol and formaldehyde, and then finally be degraded into CO_2 and H_2O.

However, for the non-normal alcohols, such as 2-propanol, the kinetic pathway is different. The non-normal alcohols react to form ketones first. Larson et al. (1995) found acetone to be the intermediate of 2-propanol PCO degradation. It is reasonable that the mechanistic scheme from 2-propanol to acetone is similar to that

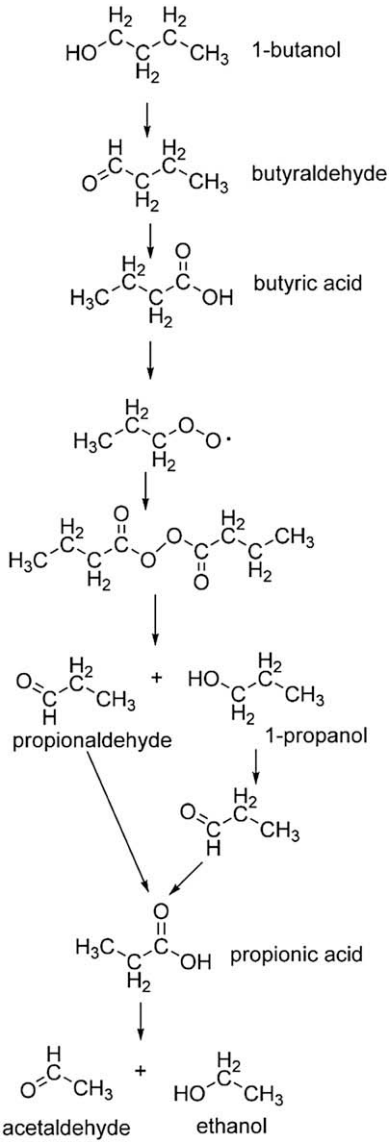

Fig. 3. Mechanistic scheme of the photocatalytic oxidation of 1-butanol.

shown by Benoit-Marquie et al. (2000). The detailed pathway of the acetone PCO process will be introduced in Section 4.2.3.

4.2.2. Aldehydes

For the simplest aldehyde, formaldehyde, formic acid was identified as its intermediate (Ao et al., 2004), in addition to carbon monoxide (Liu et al., 2005). Liu et al. (2005) summarized the detailed PCO pathway of formaldehyde over TiO_2. The other aldehydes were photocatalytically oxidized to corresponding acids, shorter carbon-chain aldehydes, carbon dioxide and water (Ye et al., 2006). Ye et al. (2006) studied the gas-phase photocatalytic oxidation of butyraldehyde and obtained its reaction pathways with active oxygen as the major oxidant: aldehydes → acids → shorter carbon-chain aldehydes. The pathways were not really the same as that discussed in Section 4.2.1. The shorter carbon-chain alkoxyalcohols were not detected in Ye's case and other alcohol PCO studies (Sauer and Ollis, 1996b; Chapuis et al., 2002). It was explained that the pathways involving hydroxyl groups (Benoit-Marquie et al., 2000) were not favored compared to the active oxygen pathways. However, Benoit-Marquie et al. reported propanol as the intermediate of propionaldehyde (see Fig. 3).

4.2.3. Ketones

Acetone is a major organic constituent of exhaled human breath and also a typical intermediate PCO product (Wisthaler et al., 2007). Attwood et al. (2003) identified an alkylperoxy species, $CH_3COCH_2OO^{\bullet}$, as the intermediate of acetone. The possible pathways are:

$$CH_3COCH_3 + O^- \rightarrow CH_3COCH_2^{\bullet} + OH^- \quad (26)$$

$$CH_3COCH_2^{\bullet} + O_2 \rightarrow CH_3COCH_2OO^{\bullet} \quad (27)$$

Raillard et al. (2006) found that the main detected intermediate was acetaldehyde, followed by methyl formate. Thus, the specie, $CH_3COCH_2OO^{\bullet}$, was possibly reacted to acetaldehyde. The pathway of acetone may be: acetone → acetaldehyde + formic acid or CO_2 → formaldehyde + methanol → formic acid. The generated formic acid and methanol might react to methyl formate, which was reported by Raillard et al. (2006). In addition, Vincent et al. (2008) detected methyl ethyl ketone (MEK) as the intermediate of acetone. They gave another explanation of the pathways: acetone → MEK → acetaldehyde.

4.2.4. Aromatics

Toluene and benzene are common indoor aromatics from paint and furniture. Benzene and toluene were found to oxidize rapidly to form adsorbed intermediates that were more strongly adsorbed and much less reactive than the original aromatics (Larson and Falconer, 1997).

4.2.4.1. Toluene. Benzaldehyde (Larson and Falconer, 1997; Mendez-Roman and Cardona-Martinez, 1998; Augugliaro et al., 1999; Marci et al., 2003; Guo et al., 2008), benzyl alcohol (Larson and Falconer, 1997; Augugliaro et al., 1999), cresol (Larson and Falconer, 1997; Marci et al., 2003), benzoic acid (Larson and Falconer, 1997; Mendez-Roman and Cardona-Martinez, 1998; Augugliaro et al., 1999), phenol (Augugliaro et al., 1999) and benzene (Augugliaro et al., 1999) were thought to be the first intermediates of toluene. Toluene reacted rapidly with O_2, but its intermediates oxidized slowly to CO_2; in contrast, benzaldehyde and benzyl alcohol were not the less reactive intermediates. The adsorbed benzaldehyde formed CO_2 at a rate that was 10 times faster than the rate that toluene formed CO_2, while benzyl alcohol reacted 20–30 times faster than toluene (Larson and Falconer, 1997). However, Blount presented another phenomenon, that there were two forms of benzaldehyde generated during the toluene PCO (Blount and Falconer, 2001). One form of benzaldehyde oxidized quickly to some less reactive intermediate, while another form of benzaldehyde with less reactivity remained on the reaction surface. In addition, benzoic acid was also not the least reactive intermediate formed during benzaldehyde PCO (Blount and Falconer, 2001). However, benzoic acid was strongly adsorbed on the reaction surface of the catalyst and was the main reason for catalyst deactivation (Mendez-Roman and Cardona-Martinez, 1998). Irokawa et al. (2006) investigated more acid intermediates on the reaction surface at about 20 ppm by diffuse reflectance Fourier-transform infrared spectroscopy (DRIFTS), such as oxalic acid, acetic acid, formic acid and pyruvic acid. Table 5 summarizes the intermediates of PCO of toluene identified in the literature.

D'hennezel et al. (1998) gave the primary toluene photocatalytic oxidation pathways. It was proposed that the hydrogen abstraction from the methyl group leads to a benzyl radical and this benzyl radical can then react with O_2 to form a benzylperoxy radical, which then self-reacts to form either benzaldehyde via a benzoxy radical or benzaldehyde and benzyl alcohol in equal amounts. Then, benzaldehyde oxidized easily into benzoic acid in the presence of O_2 and UV irradiation. Van Durme et al. (2007) introduced the degradation of toluene by non-thermal plasma discharge. Some

Table 5
Data summary for the intermediates of toluene in the literature.

Ref.	Concentration	UV source	Main intermediates	Other intermediates	Analysis method
Mendez-Roman and Cardona-Martinez, 1998	30–200 ppm	365 nm	Benzaldehyde, benzoic acid	Benzyl alcohol	FTIR, GC/MS
Augugliaro et al., 1999	400–13 000 ppm	400 W medium pressure Hg Lamp	Benzaldehyde, benzene, benzyl alcohol	Benzoic acid, phenol	FTIR, GC, HPLC
Martra et al., 1999	13 000 ppm	400 W medium pressure Hg Lamp	Benzaldehyde, benzene, benzyl alcohol, benzoic acid, phenol	–	FTIR
Maira et al., 2001	1200 ppm	–	Benzaldehyde	–	FTIR
Marci et al., 2003	0.030–0.75 mM	360 nm	Benzaldehyde	–	FTIR
Blount and Falconer, 2001		356 nm 0.3 mW cm^{-2}	Benzaldehyde	–	TPH
Blount and Falconer, 2002	100 ppm	356 nm 2.5 mW cm^{-2}	Benzaldehyde	–	TPH, TPO
Luo and Ollis, 1996	0–800 mg m^{-3}	UVP lamp	No significant intermediates	–	GC/FID
Blanco et al., 1996	3000–6000 ppm	>300 nm	Benzene, benzaldehyde	–	GC/FID, GC/MS
D'hennezel et al., 1998	13.1 ppm	365 nm	Benzoic acid, benzaldehyde, benzyl alcohol	No gas-phase intermediates	GC/FID, GC/MS, HPLC
Irokawa et al., 2006	20 ppm	Visible light	Benzaldehyde,oxalic acid, acetic acid, formic acid, pyruvic acid	No gas-phase intermediates, propionic acid, isovaleric acid, succinic acid	DRIFTS, GC, IC, GC–MS
Van Durme et al., 2007	0.5 ppm	Positive corona discharge	Formic acid, benzaldehyde, benzyl alcohol	Some nitro-products	PDMS, SPME, GC/MS/FID

HPLC: High performance liquid chromatography; DRIFTS: Diffuse reflectance Fourier-transform infrared spectroscopy; IC: Ion chromatography; PDMS: polydimethylsiloxane; SPME: solid-phase microextraction.

additional intermediates such as 4-methyl-2-propyl furan were identified and confirmed. However, the further pathways to the intermediates with few carbons were still not clear enough. Frankcombe and Smith (2007a,b) presented the results of a detailed quantum chemistry investigation of a toluene–OH–O_2 system, which was similar to the PCO process. In contrast to the pathway above, the first oxidation step of toluene was the addition of an OH radical to the toluene ring but not the methyl out of the toluene ring. They also showed the possible pathways of toluene oxidation under the OH–O_2 system (Frankcombe and Smith, 2007a).

4.2.4.2. Benzene. The major benzene intermediate was phenol, which was accompanied by hydroquinone and 1,4-benzoquinone (D'hennezel et al., 1998). Zhang et al. (2006a) got the same results and additionally found three more intermediates including 2-hexanol, 2-methylcrotonaldehyde and 4-hydroxyl-3-methyl-2-butanone. The pathways from benzene to phenol, hydroquinone and 1,4-benzoquinone were presented by D'hennezel. At high benzene concentrations, ethyl acetate and (3-methyl-oxiran-2-yl)-methanol were the two major identified intermediates, these were accompanied by butylated hydroxytoluene, 2,6-bis(1,1-dimethylethyl)-4,4-dimethylcyclohe, 2,5-cyclohexadiene-1,4,dione,2,6-bis(1,1-dim) (Zhong et al., 2007). The photocatalytic oxidation pathways of benzene were also presented in detail.

4.3. Deactivation and regeneration problems caused by intermediates

Some intermediates of the PCO process such as acids strongly adsorbed on the reaction surface (Martra et al., 1999). As discussed in Section 2.4, the adsorbed intermediates reduce the active catalyst sites. The number of active (illuminated) sites is strongly dependent on the total number of molecules converted by a photocatalyst over time. Peral et al. (1997) and Piera et al. (2002) found that the phenomena of heterogeneous catalyst deactivation can be quantified with an experimental equation like

$$\frac{r}{r_0} = \frac{1}{t^b} \tag{28}$$

where t was the time of use of the catalyst, r_0 the initial reaction rate constant obtained with a fresh catalyst, r the observed reaction rate constant at time t, and b an adjustable experimental parameter. More data was summarized by Sauer and Ollis (1996b) to show the relation among the number of active sites, total number of molecules converted and deactivation of a photocatalyst. Sauer normalized the reports in the literature by calculating the cumulative reactant conversion in units of illuminated (active) catalyst surface monolayer equivalents (meq), defined as

$$\text{meq} = \frac{\text{molecules converted}}{(\text{active})\ \text{catalyst sites}} \tag{29}$$

For single-pass fixed beds, it was found that when the contaminant conversion was higher than 1.0 meq, deactivation of the photocatalyst was reported (or noted) in 12 of the 13 studies. Huang et al. (1999) also used meq to study catalyst deactivation during photooxidation of triethylamine (TEA).

Several individual treatments or a combination of them have been reported to recover the catalyst activity. The individual treatments include (a) exposing the catalyst to pure air or humid air (D'hennezel et al., 1998; Blount and Falconer, 2002); (b) irradiating the catalyst with simultaneous UV irradiation (Einaga et al., 2001); (c) treating the catalyst with a vaporized H_2O_2 solution (Piera et al., 2002); (d) heating the surface to different temperatures (Piera et al., 2002); (e) treating the catalyst with a chlorine radical system (D'hennezel and Ollis, 1997) and (f) ozone-purging in the presence of humidity (Wang et al., 2003). Most treatments were effective, that is, the treatments worked to recover the catalyst activity. However, there were also several reports indicating that the catalyst activity degraded no matter the number or type of surface treatments (Piera et al., 2002).

5. Photocatalytic reactors

VOC removal by PCO is a surface reaction process consisting of two important steps: firstly, the VOCs have to transfer to the reaction surface; secondly, the VOCs are decomposed by the photocatalyst. Thus, the VOC convective mass transfer rate, the kinetic reaction rate and the reaction surface area are the most important performance parameters of a PCO reactor. The discussion in Section 3 emphasizes the kinetic reaction rate, but the study of PCO reactors should focus on all three parts and consider the

combined optimal effect for VOC removal, including their reactions among each other in the PCO purification process.

5.1. Mechanism model of PCO reactors

Much research has been performed on the way in which the influence factors (see Section 3) affect the PCO reactor performance (Obee and Brown, 1995; Obee, 1996; Obee and Hay, 1997; Hall et al., 1998; Yoneyama and Torimoto, 2000). Obviously, it is difficult to determine purely by experiment what influence the various factors have on VOC removal performance of PCO reactors. Modeling and simulation are also required to determine the relationship between VOC removal performance and the influencing factors. Hossain et al. (1999) combined mass transfer and kinetic reaction and firstly developed a three-dimensional convection–diffusion-reaction model for analyzing the VOC removal performance of honeycomb PCO reactors under steady-state conditions, which fitted very well with the experiments. The analysis was impressive. However, the interaction effects between the factors were still not clarified. A reduced order model for photocatalytic honeycomb reactors was described by Hall et al. (1998). The mass transfer and reaction rate limitations were also discussed by Hall.

In order to understand the interaction effects of reaction area, mass transfer, kinetic reaction rate and the other influence factors, Zhang et al. (2003), Yang et al. (2004) and Mo et al. (2005) developed a series of mechanism models. A general model was eventually developed to take into consideration the complex geometry, fluid dynamics/mass transfer and non-uniform reaction effectiveness of catalytic surfaces by Mo et al. (2005). Their analysis yielded the reactor effectiveness term (number of mass transfer units, NTU_m) which is a simple linear product of three dimensionless parameters: a geometric parameter, the Stanton number of mass transfer, and a "reaction efficiency" term. For a PCO reactor, the fractional conversion of VOC, ε was expressed as follows (Zhang et al., 2003; Mo et al., 2005):

$$\varepsilon = \frac{C_{in} - C_{out}}{C_{in}} = 1 - \exp(-NTU_m) \tag{30}$$

$$NTU_m = \frac{A_r}{A_c} St_m \eta = A^* St_m \eta \tag{31}$$

where C_{in} and C_{out} are the inlet and outlet VOC concentrations of a PCO reactor respectively; NTU_m is the number of the mass transfer unit; A_r is the reaction surface area; and A_c is the cross-sectional area.

The VOC removal bottleneck of the PCO reactor can be determined by analyzing the values of A^*, St_m, and η (Mo et al., 2008). A^* represents the geometric and structural characteristics of a PCO reactor, that is, it only depends on the geometric size of PCO reactor. St_m is the dimensionless convective mass transfer coefficient and shows the synergistic degree of alignment between the velocity and concentration fields. η describes the relative intensity between the PCO reaction rate and the mass transfer rate. η also stands for the criterion for mass transfer or kinetic reaction limits mentioned in Section 3.3. The selection of MTB or traditional method for kinetic parameter evaluation will be performed through the value of η. Both of St_m and η are positive and not greater than 1. When η is equal to 1, the ideal NTU_m (Yang et al., 2004) was obtained.

5.2. Comparison of various PCO reactors

There are various PCO reactors reported in the literature, including power layer (Peral and Ollis, 1992), plate (Obee and Hay, 1997; Mo et al., 2005; Salvado-Estivill et al., 2007; Yang et al., 2007), honeycomb (Hossain et al., 1999), annular (Jacoby et al., 1995; Doucet et al., 2006; Mo et al., 2008), packed-bed (Mehrvar et al., 2002; Alexiadis and Mazzarino, 2005; Arabatzis et al., 2005), fluidized-bed (Chen et al., 2003), optical fiber (Choi et al., 2001), mop fan (Riffat and Zhao, 2007) and combined-adsorption type (Shiraishi et al., 2003, 2007). Fig. 4 shows some reactors described in the literature.

These reactors were sorted according to the configuration of the UV lamps with respect to the reaction area. The different configurations lead to different characteristics of the reaction area, mass transfer and photocatalytic reaction. The plate, honeycomb monolith and annular are three representative types among these reactors. Table 6 summarizes the performance of some PCO reactors on formaldehyde degradation. From the three key parameters A^*, St_m, and η, the bottleneck of the reactor performance can be found. For the plate type reactor, it is possible to obtain the large convective mass transfer rate and reaction rate, but the reaction area is much smaller than other types of reactors. In the honeycomb type reactor, the UV light is parallel to the reaction area (see Fig. 4(c)), which results in low reaction rate even if the reaction area and mass transfer are large. For the annular type reactor, the convective mass transfer rate and reaction area are small, even when the UV light irradiates on the reaction area directly (see Fig. 4(f)).

Ideally, the structure of a PCO reactor should have high specific surface for a large reaction area, support small pass-through channels and low air velocity for a high mass transfer and have the UV light irradiate directly on the reaction surface. Normally, the structure of a PCO reactor consists of two parts: the reaction structure and the UV source. The reaction structure supports not only the photocatalyst carrier, but also the airflow channels. Thus, the parameters: A^* and St_m are dependent on the reaction structure. Obviously, the UV source determines η. Most PCO reactors have a separate UV source and reaction structure, which leads to the PCO process being limited by either mass transfer or kinetic reaction (Yang et al., 2004). This results in low VOC removal efficiency and an incomplete reaction. The lack of coordination of the reaction structure and the UV source make PCO reactor design difficult.

If combined with adsorption (i.e. activated carbon filter (Ao and Lee, 2005; Tao et al., 2006)), the performance of a PCO reactor was expected to improve. But the presence of the filter introduces a considerable flow resistance, and therefore a higher energy demand. Another novel design was also developed by using a PCO reactor combined with a continuous adsorption and desorption apparatus (Shiraishi et al., 2003, 2007). However, the complex structure inhibited its application.

Another interesting approach is to use UV-transparent material to form the reaction structure. Optical fibers employ bare quartz fibers as a light-transmitting support of TiO_2, which makes the UV source and reaction structure a single entity. The photocatalytic mop fan design (Fig. 4(h)) is an improvement on the optical fiber structure. However, the TiO_2 coating thickness and fiber length have significant influence on the pollutant decomposition. Wang et al. (2005) found that the photocatalytic decomposition of benzene was hampered with a TiO_2 coating thickness of greater than 23.5 μm or fiber lengths longer than 10.0 cm. A promising PCO reactor design uses UV-LED (see Section 3.1.1) to form a honeycomb structure (Yang et al., 2006). This new reactor will overcome the shortcomings of a typical honeycomb reactor and provide a high UV intensity on the reaction surface.

6. Performance evaluation of PCO air purification

HVAC (heating, ventilation and air conditioning) systems are the major energy consumers in buildings. One way to reduce the

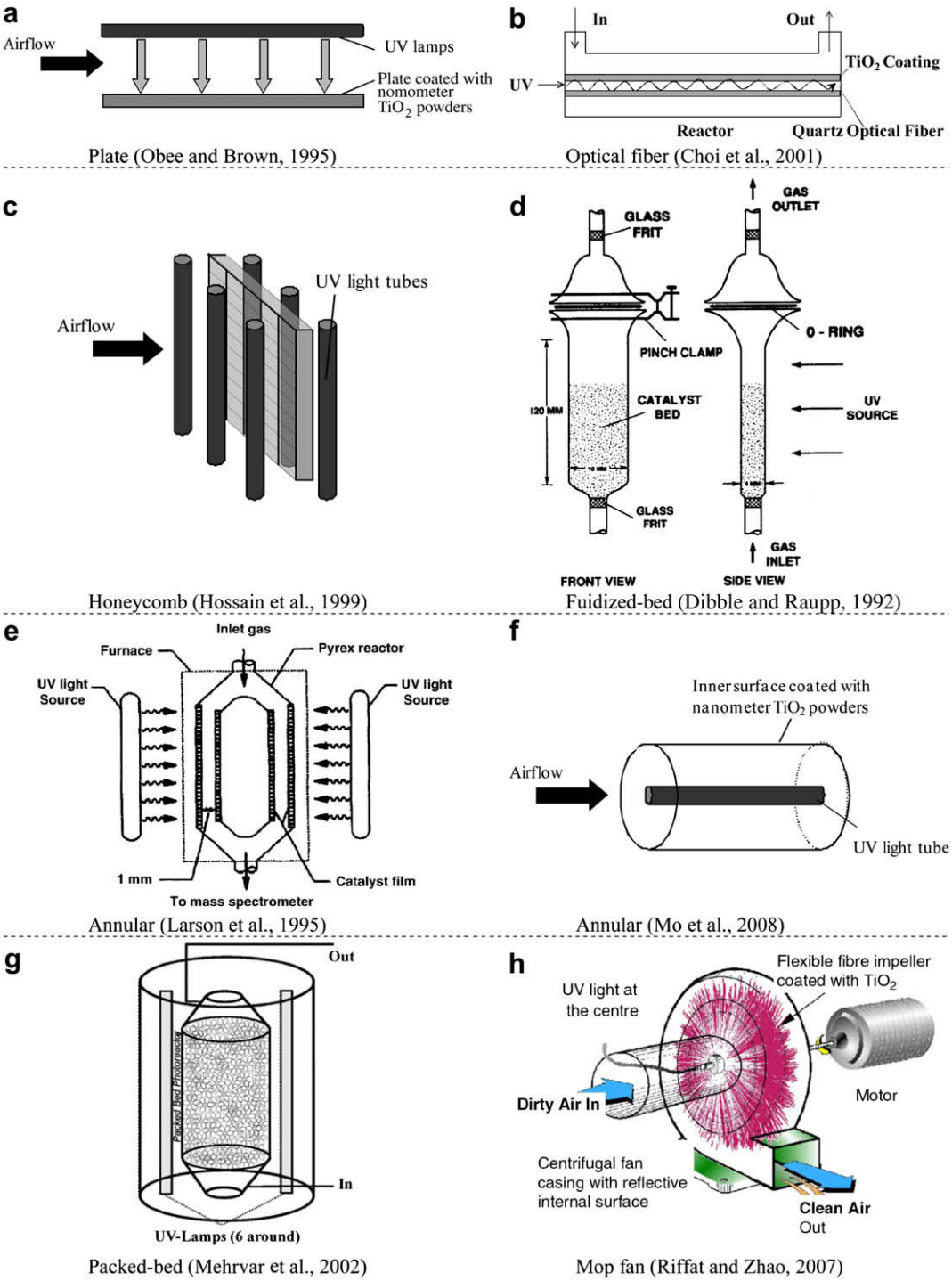

Fig. 4. Schematic of various PCO reactors. (a) Plate (Obee and Brown, 1995); (b) Optical fiber (Choi et al., 2001); (c) Honeycomb (Hossain et al., 1999); (d) Fuidized-bed (Dibble and Raupp, 1992); (e) Annular (Larson et al., 1995); (f) Annular (Mo et al., 2008); (g) Packed-bed (Mehrvar et al., 2002); (h) Mop fan (Riffat and Zhao, 2007).

energy demand of these systems would be to use a lower ventilation rate; however this could lead to problems of inadequate air quality for the building occupants. It was found that the removal of indoor air pollutants can markedly improve the perceived air quality, decreasing the ventilation rate required to achieve a given degree of acceptability (Sakr et al., 2006). Photocatalytic reactors may be integrated into new and existing HVAC systems due to their modular design, room temperature operation, and negligible pressure drop. PCO reactors also feature low power consumption and low maintenance requirements. These attributes contribute to the potential of PCO technology to be an effective process for removing and destroying low level pollutants9 in indoor air. An evaluation of PCO air purification in application is necessary to determine its performance of VOC removal.

Clean Air Deliver Rate (CADR) is typically used to evaluate the air cleaning capacity of a PCO reactor. CADR indicates the volume of purified air delivered by an air cleaner. CADR also determines how

Table 6
Performance of some PCO reactors on VOCs degradation.

Reactor	Ref.	VOC	Detail	ε (%)	NTU_m ($\times10^{-2}$)	A^*	St_m ($\times10^{-3}$)	η (%)
Honeycomb	Hossain et al., 1999; Mo et al., 2005	Formaldehyde	1 Monolith with 0.5 inch long	35.0	44.8	16.0	96.7	29.0
			2 Monolith with 0.5 inch long	52.5	85.3	32.0	77.3	34.5
			1 Monolith with 1 inch long	42.5	51.8	32.0	77.3	21.0
			2 Monolith with 1 inch long	60.5	103.0	64.0	69.0	23.3
			1 Monolith with 1.5 inch long	43.5	62.3	48.0	71.8	18.1
			2 Monolith with 1.5 inch long	66.0	115.0	96.0	66.6	18.0
Annular	Mo et al., 2008	Formaldehyde	Without fins	5.42	5.57	24.5	2.97	76.6
			With six fins	9.40	9.87	56.6	3.20	54.7
Plate	Yang et al., 2007	Formaldehyde	–	16.0	7.57	15	30.1	1.68

well an air cleaner reduces pollutants. The higher the CADR numbers, the faster the cleaner cleans the air. For a PCO air cleaner, CADR can be written as (Mo et al., 2005):

$$\mathrm{CADR} = G \times \varepsilon \tag{32}$$

where G is the airflow rate of the PCO air cleaner, ε is the fractional conversion of the VOC. Obviously, different CADR numbers could be obtained for various VOCs based on Eq. (32).

However, CADR numbers cannot describe the negative health effect of the intermediates generated by PCO (see Section 4). As we know, there are no parameters or numbers to evaluate the health-related effects of PCO intermediates so far. But, a ratio between concentrations had been developed to evaluate the health-related effect for all VOC emissions from building products (AgBB, 2008). For the evaluation of each compound i, the ratio R_i was established as defined in Eq. (33).

$$R_i = \frac{C_i}{\mathrm{LCI}_i} \tag{33}$$

where C_i is the concentration of compound i; LCI_i (Lowest Concentration of Interest) is the value qualitatively related to the health effect of compound i.

As the analogy between building products emissions and PCO intermediates, a similar Health-Related Index (HRI) would be used as the value to evaluate the performance of a PCO air cleaner. It may be defined as:

$$\mathrm{HRI}_i = \frac{C_i}{\mathrm{REL}_i} \tag{34}$$

where REL_i is the recommended exposure limit of compound i. Some institutes have published the REL values of various VOCs, such as U.S. OSHA (Occupational Safety & Health Administration) and NIOSH (National Institute for Occupational Safety and Health). It is required that HRI, the sum of all HRI_i, should not exceed the value 1. In addition, a PCO air cleaner should meet the general requirement of not generating any carcinogenic intermediates (i.e. formaldehyde, benzene).

7. Summary

A review of photocatalytic oxidation purification of indoor VOCs was performed. Although various photocatalysts with high photocatalytic activity and visible light response were prepared, relatively few investigative efforts have been made toward practical applications (i.e. indoor air cleaner or products) which may be due to the instability of these photocatalysts.

Among the various photocatalysts, TiO_2 is the most commonly used material in various PCO reactors.

Kinetic experiments and models associated with PCO reactions have been discussed. Some experimental evidence indicates that the kinetic parameters change with different reaction conditions (i.e. pollutant concentration, water vapor concentration). The kinetic model that ignores the influence of completed adsorption among all the compounds and the water vapor concentration (such as the unimolecular L–H model) would only be correct for the individual experiment. Future studies assessing kinetic parameters for photocatalysts should make a specific effort to build up the criterion evaluating their photocatalytic performance. This can be done by conforming the reaction conditions and the selected kinetic models to be consistent.

The reaction mechanisms or pathways of PCO for various VOCs are not fully understood, although parts of them had been thoroughly explained, especially for some short carbon-chain aldehydes and alcohols. Furthermore, the generated harmful intermediates (i.e. carcinogenic substances) have to be controlled. Some evidence shows that the concentrations of oxygen and hydroxyl radicals may play a significant role in the reaction pathways and the formation of different intermediates. This may lead to adjustments in the concentrations of water vapor and oxygen for reaction control. In addition, few studies have been done on the intermediates of multi-compounds. The synthetical effect of PCO is also not understood clearly when multi-VOCs are present. This shortcoming inhibits the promotion of PCO purification for the real indoor environment.

The VOC removal bottleneck of the PCO reactor can be determined by analyzing the dimensionless parameters discussed above. Problems associated with the lack of coordination of the reaction structure and the UV sources make it difficult to design a high-efficiency PCO reactor. It may be the trend to use the UV-transparent material to build up a PCO reactor. Combining UV-LED and a honeycomb structure will make a novel PCO reactor with a larger reaction area, higher mass transfer rate and higher reaction rate.

8. Future trends

The future trends for PCO purification of VOC in indoor air would include:

- Develop more stable and reliable photocatalysts that can be used in practical engineering;
- Develop hydrophobic photocatalysts in order to inhibit the negative effect of water vapor on the reaction surface;
- Understand and control the production of intermediates of some typical indoor VOCs;
- Develop a novel PCO reactor with integrated UV-LED source and reaction structure.

PCO is a promising technology for the removal of VOCs in indoor air. Current needs for indoor air purification will provide opportunities for further development of PCO in the indoor environment field.

Acknowledgements

We gratefully acknowledge the support of National Nature Science Foundation of China (grant nos. 50436040 and 50725620)

and National 11th Five-Year Plan of Dept. of Science, China (grant no. 2006BAJ02A08).

References

AgBB, 2008. Health-related Evaluation Procedure for Volatile Organic Compounds Emissions (VOC and SVOC) from Building Products. Committee for Health-related Evaluation of Building Products.

Alberici, R.M., Jardim, W.E., 1997. Photocatalytic destruction of VOCs in the gas-phase using titanium dioxide. Applied Catalysis B – Environmental 14, 55–68.

Alexiadis, A., Mazzarino, I., 2005. Design guidelines for fixed-bed photocatalytic reactors. Chemical Engineering and Processing 44, 453–459.

Ao, C.H., Lee, S.C., 2004. Combination effect of activated carbon with TiO_2 for the photodegradation of binary pollutants at typical indoor air level. Journal of Photochemistry and Photobiology A – Chemistry 161, 131–140.

Ao, C.H., Lee, S.C., 2005. Indoor air purification by photocatalyst TiO_2 immobilized on an activated carbon filter installed in an air cleaner. Chemical Engineering Science 60, 103–109.

Ao, C.H., Lee, S.C., Yu, J.Z., Xu, J.H., 2004. Photodegradation of formaldehyde by photocatalyst TiO_2: effects on the presences of NO, SO_2 and VOCs. Applied Catalysis B – Environmental 54, 41–50.

Arabatzis, I.M., Spyrellis, N., Loizos, Z., Falaras, P., 2005. Design and theoretical study of a packed bed photoreactor. Journal of Materials Processing Technology 161, 224–228.

Asahi, R., Morikawa, T., Ohwaki, T., Aoki, K., Taga, Y., 2001. Visible-light photocatalysis in nitrogen-doped titanium oxides. Science 293, 269–271.

Attwood, A.L., Edwards, J.L., Rowlands, C.C., Murphy, D.M., 2003. Identification of a surface alkylperoxy radical in the photocatalytic oxidation of acetone/O-2 over TiO_2. Journal of Physical Chemistry A 107, 1779–1782.

Augugliaro, V., Coluccia, S., Loddo, V., Marchese, L., Martra, G., Palmisano, L., Schiavello, M., 1999. Photocatalytic oxidation of gaseous toluene on anatase TiO_2 catalyst: mechanistic aspects and FT-IR investigation. Applied Catalysis B – Environmental 20, 15–27.

Auvinen, J., Wirtanen, L., 2008. The influence of photocatalytic interior paints on indoor air quality. Atmospheric Environment 37, 4101–4112.

Belver, C., Lopez-Munoz, M.J., Coronado, J.M., Soria, J., 2003. Palladium enhanced resistance to deactivation of titanium dioxide during the photocatalytic oxidation of toluene vapors. Applied Catalysis B – Environmental 46, 497–509.

Benoit-Marquie, F., Wilkenhoner, U., Simon, V., Braun, A.M., Oliveros, E., Maurette, M.T., 2000. VOC photodegradation at the gas–solid interface of a TiO_2 photocatalyst – Part I: 1-butanol and 1-butylamine. Journal of Photochemistry and Photobiology A – Chemistry 132, 225–232.

Bhattacharyya, A., Kawi, S., Ray, M.B., 2004. Photocatalytic degradation of orange II by TiO_2 catalysts supported on adsorbents. Catalysis Today 98, 431–439.

Biard, P.F., Bouzaza, A., Wolbert, D., 2007. Photocatalytic degradation of two volatile fatty acids in an annular plug-flow reactor; kinetic modeling and contribution of mass transfer rate. Environmental Science & Technology 41, 2908–2914.

Blanco, J., Avila, P., Bahamonde, A., Alvarez, E., Sanchez, B., Romero, M., 1996. Photocatalytic destruction of toluene and xylene at gas phase on a titania based monolithic catalyst. Catalysis Today 29, 437–442.

Blount, M.C., Falconer, J.L., 2001. Characterization of adsorbed species on TiO_2 after photocatalytic oxidation of toluene. Journal of Catalysis 200, 21–33.

Blount, M.C., Falconer, J.L., 2002. Steady-state surface species during toluene photocatalysis. Applied Catalysis B – Environmental 39, 39–50.

Bosc, F., Edwards, D., Keller, N., Keller, V., Ayral, A., 2006. Mesoporous TiO_2-based photocatalysts for UV and visible light gas-phase toluene degradation. Thin Solid Films 495, 272–279.

Bouzaza, A., Vallet, C., Laplanche, A., 2006. Photocatalytic degradation of some VOCs in the gas phase using an annular flow reactor – determination of the contribution of mass transfer and chemical reaction steps in the photodegradation process. Journal of Photochemistry and Photobiology A – Chemistry 177, 212–217.

Brezova, V., Blazkova, A., Karpinsky, L., Groskova, J., Havlinova, B., Jorik, V., Ceppan, M., 1997. Phenol decomposition using $Mn+/TiO_2$ photocatalysts supported by the sol–gel technique on glass fibres. Journal of Photochemistry and Photobiology A – Chemistry 109, 177–183.

Chang, C.P., Chen, J.N., Lu, M.C., 2003. Heterogeneous photocatalytic oxidation of acetone for air purification by near UV-irradiated titanium dioxide. Journal of Environmental Science and Health Part A – Toxic/Hazardous Substances & Environmental Engineering 38, 1131–1143.

Changrani, R., Raupp, G.B., 1999. Monte Carlo simulation of the radiation field in a reticulated foam photocatalytic reactor. AIChE Journal 45, 1085–1094.

Chapuis, Y., Kivana, D., Guy, C., Kirchnerova, J., 2002. Photocatalytic oxidation of volatile organic compounds using fluorescent visible light. Journal of the Air & Waste Management Association 52, 845–854.

Chen, D.H., Ye, X.J., Li, K.Y., 2005. Oxidation of PCE with a UV LED photocatalytic reactor. Chemical Engineering & Technology 28, 95–97.

Chen, F., Zhao, J.C., Hidaka, H., 2003. Adsorption factor and photocatalytic degradation of dye-constituent aromatics on the surface of TiO_2 in the presence of phosphate anions. Research on Chemical Intermediates 29, 733–748.

Chen, H.Y., Zahraa, O., Bouchy, M., 1997. Inhibition of the adsorption and photocatalytic degradation of an organic contaminant in an aqueous suspension of TiO_2 by inorganic ions. Journal of Photochemistry and Photobiology A – Chemistry 108, 37–44.

Chen, W.H., Zhang, J.S., 2008. Photocatalytic oxidation of multi-component systems – an investigation using toluene/ethylbenzene, octane/decane/dodecane and formaldehyde/acetaldehyde. Journal of Advanced Oxidation Technologies 11, 163–173.

Cheng, H., Ma, J., Zhao, Z., Qi, L., 1995. Hydrothermal preparation of uniform nanosize rutile and anatase particles. Chemistry of Materials 7, 663–671.

Choi, W., Ko, J.Y., Park, H., Chung, J.S., 2001. Investigation on TiO_2-coated optical fibers for gas-phase photocatalytic oxidation of acetone. Applied Catalysis B – Environmental 31, 209–220.

Choi, W.Y., Termin, A., Hoffmann, M.R., 1994. The role of metal-ion dopants in quantum-sized TiO_2 – correlation between photoreactivity and charge-carrier recombination dynamics. Journal of Physical Chemistry 98, 13669–13679.

Choung, J.H., Lee, Y.W., Choi, D.K., Kim, S.H., 2001. Adsorption equilibria of toluene on polymeric adsorbents. Journal of Chemical and Engineering Data 46, 954–958.

Coronado, J.M., Zorn, M.E., Tejedor-Tejedor, I., Anderson, M.A., 2003. Photocatalytic oxidation of ketones in the gas phase over TiO_2 thin films: a kinetic study on the influence of water vapor. Applied Catalysis B – Environmental 43, 329–344.

D'hennezel, O., Ollis, D.F., 1997. Trichloroethylene-promoted photocatalytic oxidation of air contaminants. Journal of Catalysis 167, 118–126.

D'hennezel, O., Pichat, P., Ollis, D.F., 1998. Benzene and toluene gas-phase photocatalytic degradation over H_2O and HCL pretreated TiO_2: by-products and mechanisms. Journal of Photochemistry and Photobiology A – Chemistry 118, 197–204.

Dibble, L.A., Raupp, G.B., 1992. Fluidized-bed photocatalytic oxidation of trichloroethylene in contaminated airstreams. Environmental Science & Technology 26, 492–495.

Doucet, N., Bocquillon, F., Zahraa, O., Bouchy, M., 2006. Kinetics of photocatalytic VOCs abatement in a standardized reactor. Chemosphere 65, 1188–1196.

Drelich, J., Lu, Y.Q., Chen, L.Y., Miller, J.D., Guruswamy, S., 1998. FTIR internal reflection spectroscopy studies of the effect of pH on adsorption of oleate oleic acid at the surface of a TiO_2 thin film deposited on a Ge single crystal. Applied Surface Science 125, 236–244.

Egerton, T.A., King, C.J., 1979. The influence of light intensity on photoactivity on TiO_2 pigmented systems. Journal of the Oil & Colour Chemists Association 62, 386–391.

Einaga, H., Futamura, S., Ibusuki, T., 2001. Complete oxidation of benzene in gas phase by platinized titania photocatalysts. Environmental Science & Technology 35, 1880–1884.

Fisk, W.J., Rosenfeld, A.H., 1997. Estimates of improved productivity and health from better indoor environments. Indoor Air 7, 158–172.

Frankcombe, T.J., Smith, S.C., 2007a. OH-initiated oxidation of toluene. 1. Quantum chemistry investigation of the reaction path. Journal of Physical Chemistry A 111, 3686–3690.

Frankcombe, T.J., Smith, S.C., 2007b. OH-initiated oxidation of toluene. 2. Master equation simulation of toluene oxide isomerization. Journal of Physical Chemistry A 111, 3691–3696.

Fu, X.Z., Clark, L.A., Yang, Q., Anderson, M.A., 1996a. Enhanced photocatalytic performance of titania-based binary metal oxides: TiO_2/SiO_2 and TiO_2/ZrO_2. Environmental Science & Technology 30, 647–653.

Fu, X.Z., Clark, L.A., Zeltner, W.A., Anderson, M.A., 1996b. Effects of reaction temperature and water vapor content on the heterogeneous photocatalytic oxidation of ethylene. Journal of Photochemistry and Photobiology A – Chemistry 97, 181–186.

Fujishima, A., Honda, K., 1972. Electrochemical photolysis of water at a semiconductor electrode. Nature 238, 37–38.

Fujishima, A., Zhang, X.T., 2006. Titanium dioxide photocatalysis: present situation and future approaches. Comptes Rendus Chimie 9, 750–760.

Golubko, N.V., Yanovskaya, M.I., Romm, I.P., Ozerin, A.N., 2001. Hydrolysis of titanium alkoxides: thermochemical, electron microscopy, SAXS studies. Journal of Sol–Gel Science and Technology 20, 245–262.

Grinshpun, S.A., Mainelis, G., Trunov, M., Adhikari, A., Reponen, T., Willeke, K., 2005. Evaluation of ionic air purifiers for reducing aerosol exposure in confined indoor spaces. Indoor Air 15, 235–245.

Guo, T., Bai, Z.P., Wu, C., Zhu, T., 2008. Influence of relative humidity on the photocatalytic oxidation (PCO) of toluene by TiO_2 loaded on activated carbon fibers: PCO rate and intermediates accumulation. Applied Catalysis B – Environmental 79, 171–178.

Guo, W.L., Lin, Z.M., Wang, X.K., Song, G.Z., 2003. Sonochemical synthesis of nanocrystalline TiO_2 by hydrolysis of titanium alkoxides. Microelectronic Engineering 66, 95–101.

Guo, Y., Zhang, X.W., Han, G.R., 2006. Investigation of structure and properties of N-doped TiO_2 thin films grown by APCVD. Materials Science and Engineering B – Solid State Materials for Advanced Technology 135, 83–87.

Hager, S., Bauer, R., 1999. Heterogeneous photocatalytic oxidation of organics for air purification by near UV irradiated titanium dioxide. Chemosphere 38, 1549–1559.

Hall, R.T., Bendfeldt, P., Obee, T.N., Sangiovanni, J.J., 1998. Computational and experimental studies of UV/titania photocatalytic oxidation of VOCs in honeycomb monoliths. Journal of Advanced Oxidation Technologies 3, 243–251.

Hansel, A., Jordan, A., Warneke, C., Holzinger, R., Lindinger, W., 1998. Improved detection limit of the proton-transfer reaction mass spectrometer: on-line monitoring of volatile organic compounds at mixing ratios of a few PPTV. Rapid Communications in Mass Spectrometry 12, 871–875.

Hoffmann, M.R., Martin, S.T., Choi, W.Y., Bahnemann, D.W., 1995. Environmental applications of semiconductor photocatalysis. Chemical Reviews 95, 69–96.
Hossain, M.M., Raupp, G.B., Hay, S.O., Obee, T.N., 1999. Three-dimensional developing flow model for photocatalytic monolith reactors. AIChE Journal 45, 1309–1321.
Huang, A.M., Cao, L.X., Chen, J., Spiess, F.J., Suib, S.L., Obee, T.N., Hay, S.O., Freihaut, J.D., 1999. Photocatalytic degradation of triethylamine on titanium oxide thin films. Journal of Catalysis 188, 40–47.
Ihara, T., Miyoshi, M., Iriyama, Y., Matsumoto, O., Sugihara, S., 2003. Visible-light-active titanium oxide photocatalyst realized by an oxygen-deficient structure and by nitrogen doping. Applied Catalysis B – Environmental 42, 403–409.
Irie, H., Watanabe, Y., Hashimoto, K., 2003. Nitrogen-concentration dependence on photocatalytic activity of $TiO_{2-x}N_x$ powders. Journal of Physical Chemistry B 107, 5483–5486.
Irokawa, Y., Morikawa, T., Aoki, K., Kosaka, S., Ohwaki, T., Taga, Y., 2006. Photodegradation of toluene over $TiO_{2-x}N_x$ under visible light irradiation. Physical Chemistry Chemical Physics 8, 1116–1121.
Jacoby, W.A., Blake, D.M., Noble, R.D., Koval, C.A., 1995. Kinetics of the oxidation of trichloroethylene in air via heterogeneous photocatalysis. Journal of Catalysis 157, 87–96.
Kamat, P.V., Meisel, D., 2002. Nanoparticles in advanced oxidation processes. Current Opinion in Colloid & Interface Science 7, 282–287.
Khan, S.U.M., Al-Shahry, M., Ingler, W.B., 2002. Efficient photochemical water splitting by a chemically modified n-TiO_2. Science 297, 2243–2245.
Kim, S.B., Hong, S.C., 2002. Kinetic study for photocatalytic degradation of volatile organic compounds in air using thin film TiO_2 photocatalyst. Applied Catalysis B – Environmental 35, 305–315.
Kim, Y.M., Harrad, S., Harrison, R.M., 2001. Concentrations and sources of VOCs in urban domestic and public microenvironments. Environmental Science & Technology 35, 997–1004.
Kirchnerova, J., Cohen, M.L.H., Guy, C., Klvana, D., 2005. Photocatalytic oxidation of n-butanol under fluorescent visible light lamp over commercial TiO_2 (Hombicat UV100 and Degussa P25). Applied Catalysis A – General 282, 321–332.
Larson, S.A., Falconer, J.L., 1997. Initial reaction steps in photocatalytic oxidation of aromatics. Catalysis Letters 44, 57–65.
Larson, S.A., Widegren, J.A., Falconer, J.L., 1995. Transient studies of 2-propanol photocatalytic oxidation on titania. Journal of Catalysis 157, 611–625.
Lewandowski, M., Ollis, D.F., 2003a. Extension of a two-site transient kinetic model of TiO_2 deactivation during photocatalytic oxidation of aromatics: concentration variations and catalyst regeneration studies. Applied Catalysis B – Environmental 45, 223–238.
Lewandowski, M., Ollis, D.F., 2003b. A two-site kinetic model simulating apparent deactivation during photocatalytic oxidation of aromatics on titanium dioxide (TiO_2). Applied Catalysis B – Environmental 43, 309–327.
Li, L., Gu, J., Zhang, Y., 2007. Visible-light photodegradation of Rhodamine B on carbon doped titanium oxide thin film prepared by atmospheric MOCVD. Advanced Materials Research 26–28, 633–636.
Li, X.Z., Li, F.B., Xie, Y.B., 2005. Photocatalytic oxidation using lanthanide ion-doped titanium dioxide catalysts for water and wastewater treatment. Trends in Water Pollution Research, 31–74.
Li, X.Z., Li, F.B., Yang, C.L., Ge, W.K., 2001. Photocatalytic activity of WO_x–TiO_2 under visible light irradiation. Journal of Photochemistry and Photobiology A – Chemistry 141, 209–217.
Little, J.C., Hodgson, A.T., Gadgil, A.J., 1994. Modeling emissions of volatile organic-compounds from new carpets. Atmospheric Environment 28, 227–234.
Liu, H.M., Lian, Z.W., Ye, X.J., Shangguan, W.F., 2005. Kinetic analysis of photocatalytic oxidation of gas-phase formaldehyde over titanium dioxide. Chemosphere 60, 630–635.
Livage, J., 1991. Vanadium pentoxide gels. Chemistry of Materials 3, 578–593.
Luo, Y., Ollis, D.F., 1996. Heterogeneous photocatalytic oxidation of trichloroethylene and toluene mixtures in air: kinetic promotion and inhibition, time-dependent catalyst activity. Journal of Catalysis 163, 1–11.
Maira, A.J., Coronado, J.M., Augugliaro, V., Yeung, K.L., Conesa, J.C., Soria, J., 2001. Fourier transform infrared study of the performance of nanostructured TiO_2 particles for the photocatalytic oxidation of gaseous toluene. Journal of Catalysis 202, 413–420.
Maira, A.J., Yeung, K.L., Lee, C.Y., Yue, P.L., Chan, C.K., 2000. Size effects in gas-phase photo-oxidation of trichloroethylene using nanometer-sized TiO_2 catalysts. Journal of Catalysis 192, 185–196.
Marci, G., Addamo, M., Augugliaro, V., Coluccia, S., Garcia-Lopez, E., Loddo, V., Martra, G., Palmisano, L., Schiavello, M., 2003. Photocatalytic oxidation of toluene on irradiated TiO_2: comparison of degradation performance in humidified air, in water and in water containing a zwitterionic surfactant. Journal of Photochemistry and Photobiology A – Chemistry 160, 105–114.
Martra, G., Coluccia, S., Marchese, L., Augugliaro, V., Loddo, V., Palmisano, L., Schiavello, M., 1999. The role of H_2O in the photocatalytic oxidation of toluene in vapour phase on anatase TiO_2 catalyst – a FTIR study. Catalysis Today 53, 695–702.
Mehrvar, M., Anderson, W.A., Moo-Young, M., 2002. Preliminary analysis of a tellerette packed-bed photocatalytic reactor. Advances in Environmental Research 6, 411–418.
Meininghaus, R., Salthammer, T., Knoppel, H., 1999. Interaction of volatile organic compounds with indoor materials – a small-scale screening method. Atmospheric Environment 33, 2395–2401.
Mendez-Roman, R., Cardona-Martinez, N., 1998. Relationship between the formation of surface species and catalyst deactivation during the gas-phase photocatalytic oxidation of toluene. Catalysis Today 40, 353–365.
Miyauchi, M., Ikezawa, A., Tobimatsu, H., Irie, H., Hashimoto, K., 2004. Zeta potential and photocatalytic activity of nitrogen doped TiO_2 thin films. Physical Chemistry Chemical Physics 6, 865–870.
Mo, J.H., Zhang, Y.P., Yang, R., 2005. Novel insight into VOC removal performance of photocatalytic oxidation reactors. Indoor Air 15, 291–300.
Mo, J.H., Zhang, Y.P., Yang, R., Xu, Q.J., 2008. Influence of fins on formaldehyde removal in annular photocatalytic reactors. Building and Environment 43, 238–245.
Monnoyer, P., Fonseca, A., Nagy, J.B., 1995. Preparation of colloidal AGBR particles from microemulsions. Colloids and Surfaces A – Physicochemical and Engineering Aspects 100, 233–243.
Muggli, D.S., Mccue, J.T., Falconer, J.L., 1998. Mechanism of the photocatalytic oxidation of ethanol on TiO_2. Journal of Catalysis 173, 470–483.
Nam, W., Kim, J., Han, G.Y., 2002. Photocatalytic oxidation of methyl orange in a three-phase fluidized bed reactor. Chemosphere 47, 1019–1024.
Nasr, C., Vinodgopal, K., Fisher, L., Hotchandani, S., Chattopadhyay, A.K., Kamat, P.V., 1996. Environmental photochemistry on semiconductor surfaces. Visible light induced degradation of a textile diazo dye, naphthol blue black, on TiO_2 nanoparticles. Journal of Physical Chemistry 100, 8436–8442.
Noguchi, T., Fujishima, A., 1998. Photocatalytic degradation of gaseous formaldehyde using TiO_2 film. Environmental Science & Technology 32, 3831–3833.
Obee, T.N., 1996. Photooxidation of sub-parts-per-million toluene and formaldehyde levels on titania using a glass-plate reactor. Environmental Science & Technology 30, 3578–3584.
Obee, T.N., Brown, R.T., 1995. TiO_2 photocatalysis for indoor air applications – effects of humidity and trace contaminant levels on the oxidation rates of formaldehyde, toluene, and 1,3-butadiene. Environmental Science & Technology 29, 1223–1231.
Obee, T.N., Hay, S.O., 1997. Effects of moisture and temperature on the photooxidation of ethylene on titania. Environmental Science & Technology 31, 2034–2038.
Obuchi, E., Sakamoto, T., Nakano, K., Shiraishi, F., 1999. Photocatalytic decomposition of acetaldehyde over TiO_2/SiO_2 catalyst. Chemical Engineering Science 54, 1525–1530.
OEHHA, 2007. California's Office of Environmental Health Hazard Assessment. http://www.oehha.ca.gov/air.html.
Ohtani, B., 2008. Preparing articles on photocatalysis – beyond the illusions, misconceptions, and speculation. Chemistry Letters 37, 217–229.
Ollis, D.F., 2000. Photocatalytic purification and remediation of contaminated air and water. Comptes Rendus De L Academie Des Sciences Serie Ii Fascicule C-Chimie 3, 405–411.
Park, D.R., Zhang, J.L., Ikeue, K., Yamashita, H., Anpo, M., 1999. Photocatalytic oxidation of ethylene to CO_2 and H_2O on ultrafine powdered TiO_2 photocatalysts in the presence of O-2 and H_2O. Journal of Catalysis 185, 114–119.
Peral, J., Domenech, X., Ollis, D.F., 1997. Heterogeneous photocatalysis for purification, decontamination and deodorization of air. Journal of Chemical Technology and Biotechnology 70, 117–140.
Peral, J., Ollis, D.F., 1992. Heterogeneous photocatalytic oxidation of gas-phase organics for air purification: acetone, 1-butanol, butyraldehyde, formaldehyde, and m-xylene oxidation. Journal of Catalysis 136, 554–565.
Piera, E., Ayllon, J.A., Domenech, X., Peral, J., 2002. TiO_2 deactivation during gas-phase photocatalytic oxidation of ethanol. Catalysis Today 76, 259–270.
Qi, L.M., Ma, J.M., Cheng, H.M., Zhao, Z.G., 1996. Preparation of BaSO4 nanoparticles in non-ionic w/o microemulsions. Colloids and Surfaces A – Physicochemical and Engineering Aspects 108, 117–126.
Raillard, C., Hequet, V., Le Cloirec, P., Legrand, J., 2006. Photocatalytic oxidation of methyl ethyl ketone over sol–gel and commercial TiO_2 for the improvement of indoor air. Water Science and Technology 53, 107–115.
Raillard, C., Hequet, V., Le Cloirec, P., Legrand, J., 2004. Kinetic study of ketones photocatalytic oxidation in gas phase using TiO_2-containing paper: effect of water vapor. Journal of Photochemistry and Photobiology A – Chemistry 163, 425–431.
Raupp, G.B., Nico, J.A., Annangi, S., Changrani, R., Annapragada, R., 1997. Two-flux radiation-field model for an annular packed-bed photocatalytic oxidation reactor. AIChE Journal 43, 792–801.
Riffat, S.B., Zhao, X., 2007. Preliminary study of the performance and operating characteristics of a mop-fan air cleaning system for buildings. Building and Environment 42, 3241–3252.
Rubio, J., Oteo, J.L., Villegas, M., Duran, P., 1997. Characterization and sintering behaviour of submicrometre titanium dioxide spherical particles obtained by gas-phase hydrolysis of titanium tetrabutoxide. Journal of Materials Science 32, 643–652.
Ruthven, D.M., 1984. Principles of Adsorption and Adsorption Processes. Wiley, New York.
Sakr, W., Weschler, C.J., Fanger, P.O., 2006. The impact of sorption on perceived indoor air quality. Indoor Air 16, 98–110.
Salvado-Estivill, I., Brucato, A., Puma, G.L., 2007. Two-dimensional modeling of a flat-plate photocatalytic reactor for oxidation of indoor air pollutants. Industrial & Engineering Chemistry Research 46, 7489–7496.
Sanchez, B., Cardona, A.I., Romero, M., Avila, P., Bahamonde, A., 1999. Influence of temperature on gas-phase photo-assisted mineralization of TCE using tubular and monolithic catalysts. Catalysis Today 54, 369–377.
Sano, T., Negishi, N., Takeuchi, K., Matsuzawa, S., 2004. Degradation of toluene and acetaldehyde with Pt-loaded TiO_2 catalyst and parabolic trough concentrator. Solar Energy 77, 543–552.

Sauer, M.L., Hale, M.A., Ollis, D.F., 1995. Heterogeneous photocatalytic oxidation of dilute toluene–chlorocarbon mixtures in air. Journal of Photochemistry and Photobiology A – Chemistry 88, 169–178.
Sauer, M.L., Ollis, D.F., 1994. Acetone oxidation in a photocatalytic monolith reactor. Journal of Catalysis 149, 81–91.
Sauer, M.L., Ollis, D.F., 1996a. Catalyst deactivation in gas–solid photocatalysis. Journal of Catalysis 163, 215–217.
Sauer, M.L., Ollis, D.F., 1996b. Photocatalyzed oxidation of ethanol and acetaldehyde in humidified air. Journal of Catalysis 158, 570–582.
Serpone, N., Pelizzetti, E., 1989. Adsorption–desorption, related mobility and reactivity in photocatalysis. In: Photocatalysis: Fundamentals and Applications. Wiley, New York, pp. 217–250.
Shie, J.L., Lee, C.H., Chiou, C.S., Chang, C.T., Chang, C.C., Chang, C.Y., 2008. Photodegradation kinetics of formaldehyde using light sources of UVA, UVC and UVLED in the presence of composed silver titanium oxide photocatalyst. Journal of Hazardous Materials 155, 164–172.
Shiraishi, F., Nomura, T., Yamaguchi, S., Ohbuchi, Y., 2007. Rapid removal of trace HCHO from indoor air by an air purifier consisting of a continuous concentrator and photocatalytic reactor and its computer simulation. Chemical Engineering Journal 127, 157–165.
Shiraishi, F., Yamaguchi, S., Ohbuchi, Y., 2003. A rapid treatment of formaldehyde in a highly tight room using a photocatalytic reactor combined with a continuous adsorption and desorption apparatus. Chemical Engineering Science 58, 929–934.
Sobana, N., Muruganandam, M., Swantinathan, M., 2008. Characterization of AC–ZnO catalyst and its photocatalytic activity on 4-acetylphenol degradation. Catalysis Communications 9, 262–268.
Stokke, J.M., Mazyck, D.W., Wu, C.Y., Sheahan, R., 2006. Photocatalytic oxidation of methanol using silica–titania composites in a packed-bed reactor. Environmental Progress 25, 312–318.
Sun, Y., Fang, L., Wyon, D.P., Wisthaler, A., Lagercrantz, L., Strom-Tejsen, P., 2008. Experimental research on photocatalytic oxidation air purification technology applied to aircraft cabins. Building and Environment 43, 258–268.
Tao, Y., Wu, C.Y., Mazyck, D.W., 2006. Removal of methanol from pulp and paper mills using combined activated carbon adsorption and photocatalytic regeneration. Chemosphere 65, 35–42.
Tompkins, D.T., 2001. Evaluation of photocatalytic air cleaning capability: a literature review and engineering analysis. ASHARE Research Project RP-1134.
USEPA, 1990. Reducing Risk: Setting Priorities and Strategies for Environmental Protection. U.S. Environmental Protection Agency.
Van Durme, J., Dewulf, J., Sysmans, W., Leys, C., Van Langenhove, H., 2007. Abatement and degradation pathways of toluene in indoor air by positive corona discharge. Chemosphere 68, 1821–1829.
Vincent, G., Marquaire, P.M., Zahraa, O., 2008. Abatement of volatile organic compounds using an annular photocatalytic reactor: study of gaseous acetone. Journal of Photochemistry and Photobiology A – Chemistry 197, 177–189.
Vinodgopal, K., Hua, X., Dahlgren, R.L., Lappin, A.G., Patterson, L.K., Kamat, P.V., 1995. Photochemistry of Ru(bpy)(2)(dcbpy)(2+) on Al_2O_3 and TiO_2 surfaces – an insight into the mechanism of photosensitization. Journal of Physical Chemistry 99, 10883–10889.
Vorontsov, A.V., Dubovitskaya, V.P., 2004. Selectivity of photocatalytic oxidation of gaseous ethanol over pure and modified TiO_2. Journal of Catalysis 221, 102–109.
Vorontsov, A.V., Kurkin, E.N., Savinov, E.N., 1999. Study of TiO_2 deactivation during gaseous acetone photocatalytic oxidation. Journal of Catalysis 186, 318–324.
Vorontsov, A.V., Savinov, E.N., Barannik, G.B., Troitsky, V.N., Parmon, V.N., 1997. Quantitative studies on the heterogeneous gas-phase photooxidation of CO and simple VOCs by air over TiO_2. Catalysis Today 39, 207–218.
Wang, K.H., Hsieh, Y.H., Lin, C.H., Chang, C.Y., 1999. The study of the photocatalytic degradation kinetics for dichloroethylene in vapor phase. Chemosphere 39, 1371–1384.
Wang, K.H., Tsai, H.H., Hsieh, Y.H., 1998. A study of photocatalytic degradation of trichloroethylene in vapor phase on TiO_2 photocatalyst. Chemosphere 36, 2763–2773.
Wang, S.B., Ang, H.M., Tade, M.O., 2007. Volatile organic compounds in indoor environment and photocatalytic oxidation: state of the art. Environment International 33, 694–705.
Wang, W., Chiang, L.W., Ku, Y., 2003. Decomposition of benzene in air streams by UV/TiO_2 process. Journal of Hazardous Materials 101, 133–146.
Wang, W., Ku, Y., 2003. Photocatalytic degradation of gaseous benzene in air streams by using an optical fiber photoreactor. Journal of Photochemistry and Photobiology A – Chemistry 159, 47–59.
Wang, W., Ku, Y., Ma, C.M., Jeng, F.T., 2005. Modeling of the photocatalytic decomposition of gaseous benzene in a TiO_2 coated optical fiber photoreactor. Journal of Applied Electrochemistry 35, 709–714.
Wang, X.C., Yu, J.C., Chen, Y.L., Wu, L., Fu, X.Z., 2006. ZrO_2-modified mesoporous manocrystalline $TiO_{2-x}N_x$ as efficient visible light photocatalysts. Environmental Science & Technology 40, 2369–2374.
WHO, 1989. Indoor air quality: organic pollutants. Report on a WHO meeting, EURO Report and Studies, 1–70.
Wisthaler, A., Strom-Tejsen, P., Fang, L., Arnaud, T.J., Hansel, A., Mark, T.D., Wyon, D.P., 2007. PTR-MS assessment of photocatalytic and sorption-based purification of recirculated cabin air during simulated 7-h flights with high passenger density. Environmental Science & Technology 41, 229–234.
Wu, Z.B., Dong, F., Zhao, W.R., Guo, S., 2008. Visible light induced electron transfer process over nitrogen doped TiO_2 nanocrystals prepared by oxidation of titanium nitride. Journal of Hazardous Materials 157, 57–63.
Wu, Z.B., Gu, Z.L., Zhao, W.R., Wang, H.Q., 2007. Photocatalytic oxidation of gaseous benzene over nanosized TiO_2 prepared by solvothermal method. Chinese Science Bulletin 52, 3061–3067.
Yamazaki, S., Fu, X.Z., Anderson, M.A., Hori, K., 1996. Chlorinated byproducts from the photoassisted catalytic oxidation of trichloroethylene and tetrachloroethylene in the gas phase using porous TiO_2 pellets. Journal of Photochemistry and Photobiology A – Chemistry 97, 175–179.
Yamazaki, S., Fujinaga, N., Araki, K., 2001. Effect of sulfate ions for sol–gel synthesis of titania photocatalyst. Applied Catalysis A – General 210, 97–102.
Yang, L.C., Ishida, T., Yamakawa, T., Shinoda, S., 1996. Mechanistic study on dehydrogenation of methanol with [RuCl2(PR(3))(3)]-type catalyst in homogeneous solutions. Journal of Molecular Catalysis A – Chemical 108, 87–93.
Yang, R., Mo, J.H., Zhang, Y.P., Luo, Y., 2006. Patent: a kind of surface-light-source photocatalytic germicidal air purification device. P.R. China.
Yang, R., Zhang, Y.P., Xu, Q.J., Mo, J.H., 2007. A mass transfer based method for measuring the reaction coefficients of a photocatalyst. Atmospheric Environment 41, 1221–1229.
Yang, R., Zhang, Y.P., Zhao, R.Y., 2004. An improved model for analyzing the performance of photocatalytic oxidation reactors in removing volatile organic compounds and its application. Journal of the Air & Waste Management Association 54, 1516–1524.
Yates, H.M., Nolan, M.G., Sheel, D.W., Pemble, M.E., 2006. The role of nitrogen doping on the development of visible light-induced photocatalytic activity in thin TiO_2 films grown on glass by chemical vapour deposition. Journal of Photochemistry and Photobiology A – Chemistry 179, 213–223.
Ye, X.J., Chen, D., Gossage, J., Li, K.Y., 2006. Photocatalytic oxidation of aldehydes: byproduct identification and reaction pathway. Journal of Photochemistry and Photobiology A – chemistry 183, 35–40.
Yoneyama, H., Torimoto, T., 2000. Titanium dioxide/adsorbent hybrid photocatalysts for photodestruction of organic substances of dilute concentrations. Catalysis Today 58, 133–140.
Yu, J.G., Zhao, X.J., Du, J.C., Chen, W.M., 2000. Preparation, microstructure and photocatalytic activity of the porous TiO_2 anatase coating by sol–gel processing. Journal of Sol–Gel Science and Technology 17, 163–171.
Yu, K.P., Lee, G.W.M., Huang, W.M., Wu, C.C., Yang, S.H., 2006. The correlation between photocatalytic oxidation performance and chemical/physical properties of indoor volatile organic compounds. Atmospheric Environment 40, 375–385.
Zang, L., Macyk, W., Lange, C., Maier, W.F., Antonius, C., Meissner, D., Kisch, H., 2000. Visible-light detoxification and charge generation by transition metal chloride modified titania. Chemistry – A European Journal 6, 379–384.
Zeatoun, L., Feke, D., 2006. Characterization of TiO_2 smoke prepared using gas-phase hydrolysis of TiCl4. Particle & Particle Systems Characterization 22, 276–281.
Zhang, S.C., Zheng, Z.J., Wang, J.H., Chen, J.M., 2006a. Heterogeneous photocatalytic decomposition of benzene on lanthanum-doped TiO_2 film at ambient temperature. Chemosphere 65, 2282–2288.
Zhang, X.W., Zhou, M.H., Lei, L.C., 2006b. Co-deposition of photocatalytic Fe doped TiO_2 coatings by MOCVD. Catalysis Communications 7, 427–431.
Zhang, Y.P., Yang, R., Xu, Q.J., Mo, J.H., 2007. Characteristics of photocatalytic oxidation of toluene, benzene, and their mixture. Journal of the Air & Waste Management Association 57, 94–101.
Zhang, Y.P., Yang, R., Zhao, R.Y., 2003. A model for analyzing the performance of photocatalytic air cleaner in removing volatile organic compounds. Atmospheric Environment 37, 3395–3399.
Zhao, J., Yang, X.D., 2003. Photocatalytic oxidation for indoor air purification: a literature review. Building and Environment 38, 645–654.
Zheng, Y.Q., Erwei, S., Cui, S.X., Li, W.J., Hu, X.F., 2000. Hydrothermal preparation and characterization of brookite-type TiO_2 nanocrystallites. Journal of Materials Science Letters 19, 1445–1448.
Zhong, J.B., Wang, J.L., Tao, L., Gong, M.C., Liu, Z.L., Chen, Y.Q., 2007. Photocatalytic degradation of gaseous benzene over TiO_2/Sr_2CeO_4: kinetic model and degradation mechanisms. Journal of Hazardous Materials 139, 323–331.
Zorn, M.E., Tompkins, D.T., Zeltner, W.A., Anderson, M.A., 1999. Photocatalytic oxidation of acetone vapor on TiO_2/ZrO_2 thin films. Applied Catalysis B – Environmental 23, 1–8.